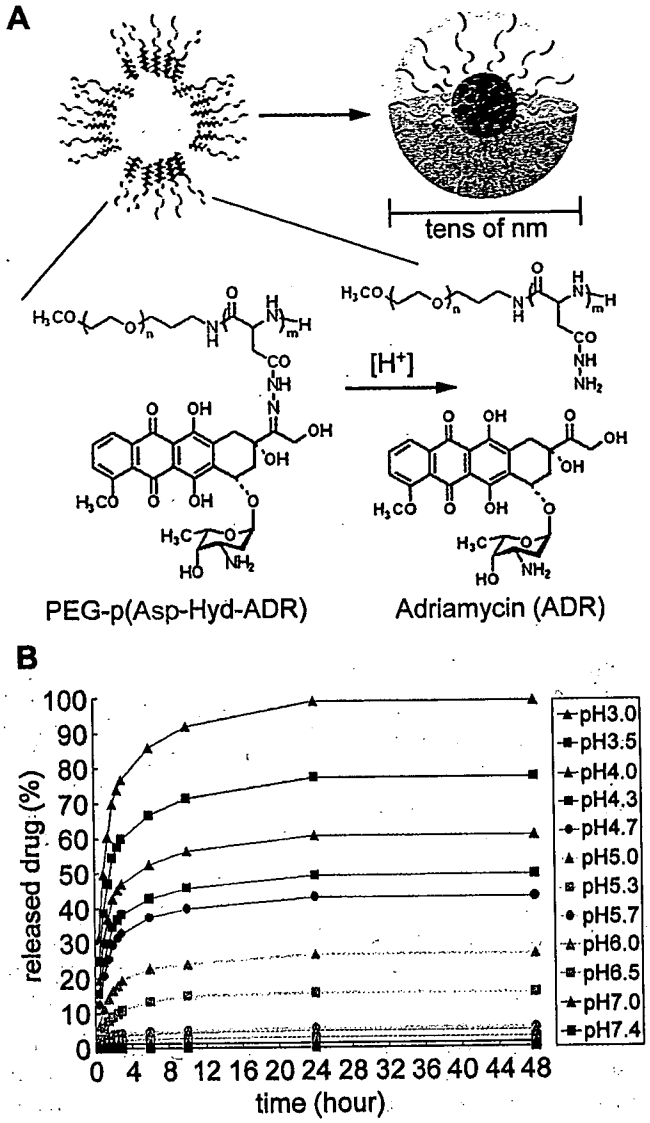

Figure 1. Preparation of tumor-infiltrating polymeric micelles with intracellular pH-sensitivity. (A) Micelles with tens of nm size diameter were prepared from self-assembling amphiphilic block copolymers, PEG-p(Asp-Hyd-ADR), in which the anticancer drug, adriamycin (ADR), was conjugated through acid-sensitive hydrazone linkers. (B) The micelles released the loaded drugs under acidic conditions below pH 6.0 corresponding to intracellular space, but remained stable under the conditions of vascular and extracellular space (pH 7.4–7.0).

conjugated to the core-forming segments through the hydrazone linkers that are stable under physiological conditions (pH 7.4) but cleavable under acidic intracellular environments in endosomes and lysosomes (pH 5–6). This carrier design allows the micelle to safely protect hydrophobic drugs from the host defense system in the body and to selectively exert cytotoxicity due to intracellular pH-triggered drug release, improving both the delivery effect and therapeutic efficacy of the drugs (*21*). Therefore, the characteristic in vitro and in vivo behaviors of the micelles would offer intriguing information taking into account the future design and development of bioresponsive supramolecular carrier systems for the intracellular trafficking of biologically active molecules.

EXPERIMENTAL PROCEDURES

Materials. β-Benzyl-L-aspartate was from Sigma and α-methoxy-ω-amino poly(ethylene glycol) (PEG; MW = 12 000) was from Nippon Oil & Fats, Japan. PEG was purified using an ion-exchange gel column (CM-Sephadex C-50, Amersham Pharmacia Biotech) prior to the synthesis of the block copolymers. Adriamycin hydrochloride-(ADR–HCl) was from Nippon Kayaku, Japan, and its purity was checked by reversed phase liquid chromatograpy (RPLC). Sephadex LH-20 gel was from Amersham Pharmacia Biotech, Sweden.

Cell Lines and Animals. A human small cell lung cancer cell line SBC-3 and murine colon adenocarcinoma 26 (C26) cells were from the National Cancer Center Research Institute, Japan, and cultured in a medium (DMEM, Sigma, St. Louis, MO) containing 10% fetal bovine serum in a humidified atmosphere with 5% CO_2 at 37 °C. CDF-1 mice (female, 6 weeks old) were from Charles River, Japan. The animals were cared for and all experiments were performed in compliance with the Guide for the Care and Use of Laboratory Animals as adopted and promulgated by the National Institutes of Health.

Preparation of the pH-Sensitive Polymeric Micelles. The self-assembling amphiphilic block copolymer, PEG-p(Asp-Hyd-ADR), was synthesized as reported elsewhere (*22*). Briefly, poly(ethylene glycol)-poly(β-benzyl-L-aspartate) (PEG-PBLA) was synthesized from the ring-opening polymerization of β-benzyl-L-aspartate *N*-carboxyanhydride using PEG as a macro initiator, followed by substitution of the benzyl groups of PEG-PBLA with hydrazide groups for drug binding (see also Supporting Information). Unbound ADR was completely removed using Sephadex LH-20 gel, and the obtained polymers were redissolved in dimethylacetamide to prepare the micelle by a dialysis method.

Evaluation of Acid-Sensitive Drug Release from the Micelles. Reversed phase liquid chromatograpy (RPLC) analysis, using a μ-Bondasphere 5 μm C4-300A column (Nihon Waters, Japan), was used to assess the pH sensitivity of the micelle. The micelle with a 10 mg/mL concentration was incubated under various buffered conditions from pH 7.4 to 3.0 [20 mM phosphate buffer (pH 7.4–6.0), 20 mM acetate buffer (pH 5.8–3.0)], and time- and pH-dependently released drugs were measured from the peak intensity by a UV detector (485 nm).

Observations on Intracellular Drug Release and Localization of the Micelles. Multicellular tumor spheroid (MCTS) was prepared from a C26 cell line using a spheroid culture plate, Sumiloncelltight (Sumitomo Bakelite, Japan); 200 μm size MCTS were sorted and used for the experiments. Fluorescence images were observed using a confocal laser scanning microscope (LSM 510, Carl Zeiss, Germany) with a 20× objective (Plan-Apochromat, Carl Zeiss, Germany) and a 63× objective (C-Apochromat, Carl Zeiss, Germany) at excitation wavelengths of 488 nm (Ar laser) and 364 nm (UV laser) for ADR and Hoechst 33258, respectively. The concentrations of the micelles in the medium were adjusted to 10 μg/mL (ADR equivalent). All images were acquired and processed with the accompanying software.

In Vitro Growth Inhibition Assay. A tetrazolium dye method, called the MTT assay, was used to evaluate the growth-inhibitory effect of the micelle. Using 96-well culture plates, exponentially growing SBC-3 cells were seeded (2000 cell/well) and preincubated for 24 h, followed by coincubation with ADR and the micelle samples. After exposure for 3, 10, and 24 h, the medium was discarded and each cell was reincubated in fresh medium for another 24 h. The cells were then counted using a Bio-RAD Microplate Reader 550 (Bio-Rad Laboratories Inc.).

In Vivo Antitumor Activity and Body Weight Change of Mice. The antitumor activity of the micelles was evaluated with tumor bearing, 7-week-old, female SPF CDF1 mice (n = 6, Charles River, Japan). After implanting C26 cells 10 days earlier, injection of the samples took place using a volume of 0.1 mL/10 g body weight. The regimens of the micelles were scheduled by changing the administration dose (20, 40, and 60 mg/kg) three times with a 4-day interval, based on the optimized regimens of ADR as a control. However, in the case of ADR, only limited doses (5, 10, and 15 mg/kg) were applied to the mice due to the drugs toxicity. The mice were monitored daily, and tumor growth and body weights were measured at 2-day intervals. Tumor volume is calculated as follows: volume = $1/2 \times LW^2$ (L is the long diameter and W is the short diameter of a tumor).

Biodistribution and Pharmacokinetics. The CDF1 mice (n = 6), when the tumor volume reached ca. 100 mm^3, were injected with ADR and the micelles in a volume of 0.1 mL/10 g body weight for the experiments. The dose was either 10 mg/kg for ADR or the micelles (ADR equivalent). After the injection, blood, tumor, and major organs (heart, kidney, liver and spleen) were collected at 0.5, 1, 3, 6, 9, 24, and 48 h, followed by HPLC anaylsis (see Supporting Information for the detailed protocol).

Fluorescence Microscopic Observations of Solid Tumors and Their Peripheral Blood Vessels. The tumor-bearing mice were sacrificed at 24 h after the injection of the micelles with a 10 mg/kg dose. The intact tumor tissues with their peripheral blood vessels were harvested for macroscopic observations using a fluorescence microscope (Axiovert 200, Carl Zeiss, Germany) equipped with a 2.5× objective (Plan-Neofluar, Carl Zeiss, Germany) and a filter set15 (BP546/12, FT580, LP590, mercury lamp excitation, Carl Zeiss, Germany).

RESULTS

Preparation of the Intracellular pH-Sensitive Polymeric Micelles. The polymer backbone of PEG-p(Asp-Hyd-ADR) consisted of poly(ethylene glycol) (PEG) with a molecular weight of 12 000 g/mol for the hydrophilic shell-forming segment and 37 repeating units of polyaspartate (PAsp) for the core-forming segment (MW = 28 679), which were determined by gel permeation chromatography and ^{1}H NMR measurements. The 28 side chains in the PAsp block were replaced by hydrazide groups for the binding of the drugs. Adriamycin (ADR) was then conjugated to the polymer backbone through hydrazone bonds between the carbonyls at the C13 of ADR and the hydrazide groups of the PEG-p(Asp-Hyd) block copolymer. Even though the biological and chemical background of binding ADR to polymer backbone through hydrazone linkages has been delineated in our previous work (*22*) as well as many studies (*23*–*26*), it must be noticed that the hydrazone linkage is the most popularly used as pH-sensitive linkers due to the fact that this bond is quite stable at pH 7.4 but hydrolyzes under mild acidic conditions with pH 5–6. Therefore, to ensure that drug release from the micelles occurs only when acid-labile hydrazone linkers are cleaved, any unbound free ADR were completely removed in this study. These were confirmed by a reversed phase liquid chromatograpy (RPLC) analysis that is generally used for separating and purifying materials due to the differences in their hydrophobic properties (further details are described below). RPLC analysis showed the drug loading content of PEG-p(Asp-Hyd-ADR) was 42.5 wt % with respect to a single block copolymer chain. The obtained PEG-p(Asp-Hyd-ADR) block copolymers self-assembled into micelles in aqueous solutions; the prepared micelles had a 65 nm diameter, which was confirmed by dynamic light scattering measurements.

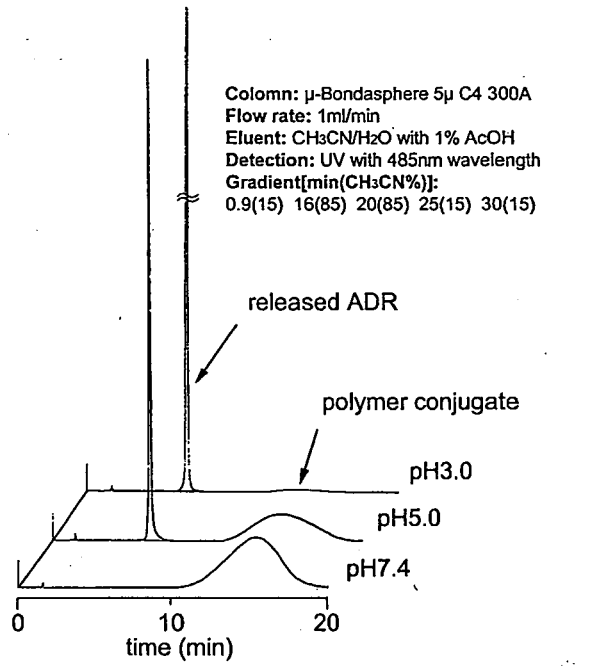

Figure 2. Acid-sensitive cleavage of drug-binding hydrazone bonds evaluated by reversed phase liquid chromatography (RPLC) analysis. RPLC separates free drugs and polymer conjugates due to the differences in their hydrophobic properties, demonstrating absence of free drugs at pH 7.4 possibly binding to polymer conjugates in a physical way. On the other hand, it clearly shows that the amount of released drugs increases under acidic conditions in which the drug-binding hydrazone linkers can be cleaved.

The Micelles Selectively Release the Loaded Drugs by Sensing a pH Decrease. To confirm the acid-sensitive drug release profile, the micelles were incubated under various pH conditions from 7.4 to 3.0, and the released drugs were measured using RPLC analysis. Figure 1B shows that the micelles released the loaded drugs time- and pH-dependently as the external pH decreased, while they were stable under physiological conditions at pH 7.4 for over 48 h. The results indicate the micelles should release the loaded drugs in the intracellular acidic regions (pH 5–6) such as endosomes and lysosomes in which the drug-binding hydrazone linkers can be cleaved most effectively. Chemical evidence for absence of free drugs and acid-sensitive cleavage of hydrazone linkers to induce drug release was also presented by RPLC analysis (Figure 2). As described above, ADR is conjugated to amphiphilic block copolymers through pH-sensitive hydrazone linkers. If the drugs were simply entrapped in the micelles by physical interaction instead binding to polymers via chemical linkers, a sharp peak corresponding to the free drug should be separated from drug–polymer conjugates by RPLC and appeared in the physiological condition (pH 7.4) where the acid-labile hydrazone bond remains stable. However, the peak from the free drug was not shown at pH 7.4 but gradually increased in acidic conditions while the broad peak from polymer conjugates decreased. Eventually, almost 100% of the drugs were released at pH 3.0, and on the basis of this, we calculated the drug loading content of polymer conjugate described above. These results demonstrate that acid-sensitive cleavage

Table 1. Growth Inhibitory Effects of the Micelles against Cancer Cells[a]

sample	exposure time (hour)	IC_{50}[b] (μg/mL±SD)	relative index[c]
ADR	3	0.041 ± 0.035	1.05
	10	0.048 ± 0.026	1.23
	24	0.039 ± 0.025	1
micelle	3	1.08 ± 0.12	27.69
	10	0.45 ± 0.061	11.54
	24	0.27 ± 0.038	6.92

[a] Eight independent experiments were carried out using a human small cell lung cancer cell line SBC-3 ($n = 8$). [b] IC_{50} denotes the inhibitory concentration of the drugs required for 50% reduction in cell population. Concentrations of the micelles are calculated with free ADR equivalents. [c] Relative index denotes the ratio between a control and the object for comparison. Here, we evaluated the growth inhibitory effect of the micelles by converting their concentrations with respect to ADR after a 24 h incubation as the control.

of hydrazone linkers between drugs and polymer chains obviously induced drug release.

Regenerated Drugs Were Pharmaceutically Active Inhibiting Cell Growth in Vitro. To verify whether the released drugs are pharmacologically active, an in vitro growth-inhibition test was carried out. The test revealed that the cytotoxic activity of the micelles was as high as 1/7-fold with respect to that of the free drugs after a 24 h exposure time (Table 1). Interestingly, the micelles showed delayed cytotoxicity that was drastically changed depending on the incubation time, which reflects that the drug release from the micelles took place and correlated with the cell metabolism.

The Micelle Infiltrates into the Avascular Tumor Model Multicellular Tumor Spheroids. Recently, it has been reported that the fluorescence quenching effect of the micelles provides a useful tool to observe the intracellular behaviors of the micelles (*22*). The fluorescence intensity of ADR, playing a role not only as an anticancer drug, but also as a fluorescence probe in this study, is quenched due to the locally increased high concentration in the micelle core; however, the fluorescence becomes detectable again as the micelles start to release ADR under acidic conditions. Consequently, the micelles emit intense fluorescence signals with the release of the entrapped ADR; a series of processes such as intracellular trafficking, drug release, and localization were able to be directly monitored in live cells accompanying the structural change. In the meantime, the multicellular tumor spheroid (MCTS) was used as an in vitro tumor model for the experiments because it is the most similar to avascular tumor regions of practical solid tumors in vivo that are characterized by limited accessibility of cell subpopulations (Figure 3). For example, MCTS reproduces adverse microenvironmental conditions of solid tumors in vivo such as hypoxia and nutritional depletion, and the extracellular matrix between tumor cells instead of intratumoral normal cell populations (*27*–*28*).

For these reasons, the intracellular behaviors of the micelles were observed within solid tumors using fluorescence quenching effect and the MCTS. The micelles were coincubated with the MCTS, and the change in the fluorescence intensity was monitored using a confocal laser scanning microscope (CLSM). The three-dimensional CLSM images demonstrated the time-dependent change in the fluorescence intensity of the micelle systems and their distributions throughout the MCTS with a 200 μm diameter depending on the incubation time (Figure 4A). The 200 μm diameter of MCTS was

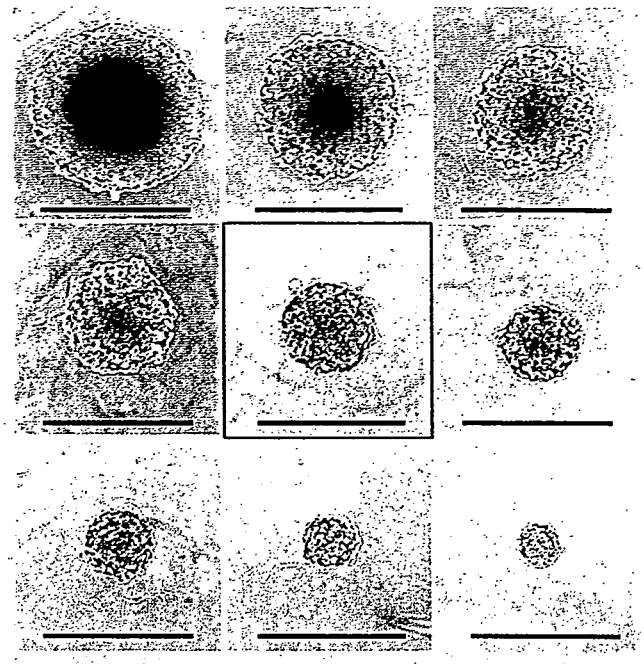

Figure 3. Preparation of multicellular tumor spheroid (MCTS). MCTS with diameter ranging from 100 to 500 μm was prepared from a C26 cell line. Among them, MCTS with a 200 μm diameter (red-edged) was used as an in vitro tumor model because it has the most suitable size for reproducing in vivo avascular tumor regions that are characterized by limited accessibility of cell subpopulations (bar = 500 μm).

determined as the most suitable size for the experiments, considering the fact that the maximum distance between the capillary blood vessels within avascular solid tumor is 200 μm or less (*29*). The fluorescence of the micelle system remained quenched at 1 h after incubation, but it was detected at 3 and 24 h. It is notable that most cell nuclei remained blue at 3 h. The images, therefore, suggest that the micelles began to intracellularly release the drugs but the released drugs were still localized in the cytoplasm. However, the intense fluorescence of ADR was eventually detected in most of the cell nuclei after 24 h. These results reflect that the micelles would access every cell in the avascular region of tumor tissues in vivo to release the drugs.

The Micelles Enter the Cell Interior and Release the Drugs. To get a better understanding of the intracellular distributions of the micelles and their released drugs, further observations of the MCTS coincubated with the micelles under high magnification were carried out using a 63× objective (Figure 4B). These images show clear evidence of the intracellular drug release from the micelles and accumulation of the released drugs in the cell nuclei. The localization of the ADR fluorescence in the cytoplasm after 3 h incubation is supporting our speculation that the micelles internalized the cells releasing the drugs. After additional incubation up to 24 h, the presence of the drugs both in the cytoplasm and cell nuclei was confirmed. When the same experiments were carried out with free ADR, all the cell nuclei in the MCTS became red within 1 h because the ADR with a low molecular weight rapidly penetrated into each cell, and we were not able to observe this unique time-dependent fluorescence change in intensity and its distribution. Therefore, it is obvious that the micelles are precisely functioning in the intracellular regions as we designed, and the possible drug release from the micelles in the extracellular regions is negligible.

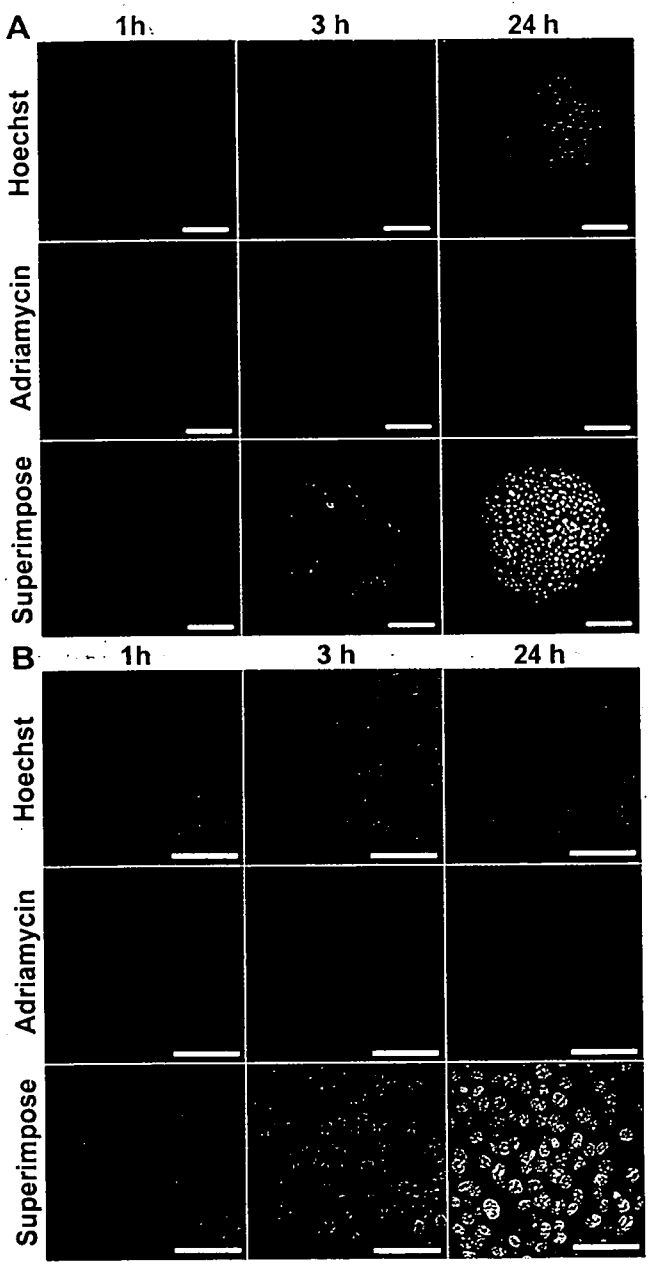

Figure 4. Observation of tumor permeability and intracellular drug release behaviors of the micelles. (A) CLSM observations showed the time-dependent change in the fluorescence intensities of ADR in the micelle system in MCTS. The images showed that the micelles can access the inside of the MCTS and release the loaded drugs (bar = 100 μm). (B) The intracellular drug release and localization of the micelles in each cell of MCTS were observed in detail using a high-magnification 63× objective. The images clearly demonstrated that the micelles internalized into the cells and released drugs, and that the released drugs eventually accumulated in the cell nuclei (bar = 50 μm).

The Micelles Suppress Tumor Growth in Mice with Enhanced Therapeutic Efficacy and Lowered Toxicity. The animal tests revealed that the micelles exerted an effective antitumor activity over a broad range of injection doses to suppress tumor growth in mice, showing some of the clear comparisons with ADR (Figure 5). In the case of ADR, tumor growth was suppressed with a 10 mg/kg dose, but the mice treated with a 15 mg/kg dose were dead due to the drug's toxicity. This corresponds well to the fact that the lethal dose of ADR killing 50% of the test animals within a designated period, called LD_{50}, is generally 12.7−13.2 mg/kg. On the contrary, the micelles were safely injectable up to a 40 mg/kg dose, while three of six mice were completely cured and there was no death among the treated mice. Notably, the body weights of the mice that slightly decreased during the micelle administration recovered, or even increased, on day 30 with respect to the controls (Table 2). Such behavior was not observed in the case of ADR, and the mice were emaciated with a 10 mg/kg dose that was the optimum dose for ADR to suppress tumor growth. Namely, the therapeutic efficacy of the micelles was significantly improved over that of ADR within this animal experiment setting, which distinguishes the micelles from ADR that has a narrow therapeutic window between 10 and 15 mg/kg. In the meantime, the tumor-suppressing antitumor activity of the micelles is shown from a 20 mg/kg dose. The micelles also extended the duration of tumor growth reaching a 5-fold initial tumor volume up to 22 and 28 days for the 20 and 40 mg/kg doses, respectively. These results indicate that the micelles achieved both enhanced therapeutic efficacy and a reduced toxicity of the loaded drugs, which are of great advantage to create effective and safe drug carrier systems.

Table 2. In Vivo Antitumor Activity of the Micelles against C26 Tumor-Bearing Mice

sample	dose (mg/kg)[a]	body weight change on day 30 (%)[b]	toxic death	duration days of tumor growth[c]	complete cure
control	0	−2.18 ± 1.74	0/6	3.7	0/6
ADR	5	−13.35 ± 0.59	0/6	4.2	0/6
	10	−16.84 ± 1.26	0/6	14.6	1/6
	15	−	6/6	−	−
micelle	5	−0.89 ± 1.68	0/6	3.9	0/6
	10	−4.51 ± 1.44	0/6	4.0	0/6
	20	3.13 ± 1.60	0/6	22.1	2/6
	40	−4.07 ± 0.92	0/6	27.9	3/6
	60	−	6/6	−	−

[a] Administrations were carried out three times with a 4-day interval, and doses were determined in free ADR equivalents. [b] Body weights were measured on day 30 after the first injection to compare the long-term toxicity between ADR and the micelles. Values are expressed as mean ± SEM. [c] Duration time to reach 5-fold initial tumor volume.

The Micelles Circulate for a Long Time in the Blood and Selectively Accumulate in Solid Tumors. Effective antitumor activity and low toxicity imply that the micelles are stable in the blood without drug release (or leakage); therefore, their systemic and local distribution may dominate the tumor-suppressing antitumor activity. To demonstrate this, we investigated the in vivo dispositions of the micelles in detail using a biodistribution study. The levels of the micelles in the blood, tumor, and major organs, such as the heart, kidney, liver, and spleen, are expressed as percentage of each dose at specific times after the intravenous injection (Figure 6A). As summarized in Table 3, the micelles circulated in the blood for a prolonged time, and the area under the concentration curve (AUC) of the blood was 15-fold greater than that of ADR. In particular, it is noteworthy that the AUC values of the micelles in the heart and kidney decreased as compared to ADR, indicating that their tumor selectivity (AUC_{tumor}/AUC_{organ}) increased 6- and 5-fold higher with respect to the heart and the kidney, respectively. Such tumor-selective accumulation of the micelles may reduce the side effects of ADR such as cardiotoxicity and nephrotoxicity. In the meantime, the micelles showed a relatively low uptake in the liver and spleen despite the long residence time in the blood in comparison with tumors. These results suggest that the micelles may rapidly evacuate from these reticular

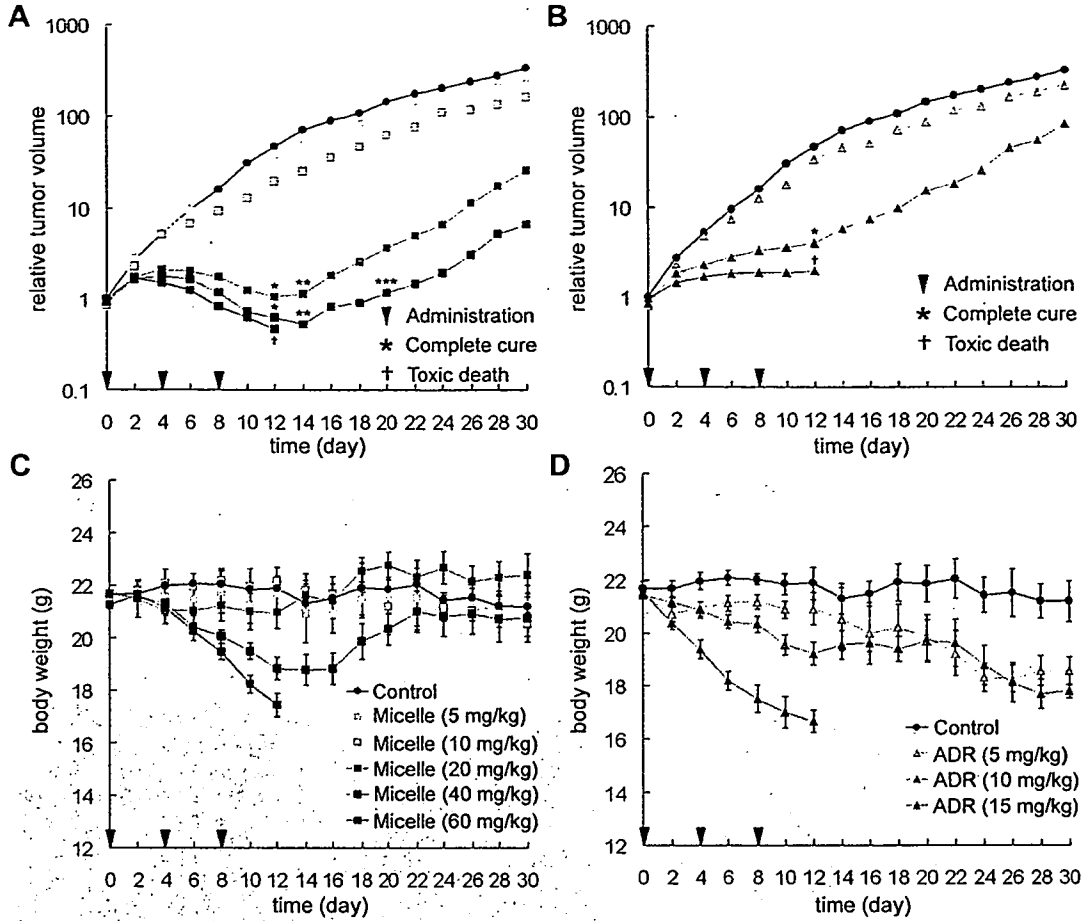

Figure 5. Tumor size and body weight changes of the treated mice. The figures show effective tumor-suppressing activity and low change in body weights over a broad range of injection doses of the micelles (A and C). To the contrary, ADR showed a narrow therapeutic window between 10 and 15 mg/kg does avoiding toxic death (B and D). Administrations were carried out three times with a 4-day interval into tumor bearing CDF1 mice (female, 6-week-old, $n = 6$). The micelle doses are shown as ADR equivalents. Values are expressed as mean and mean ± SEM for the tumor volume and body weight, respectively.

connective tissues without interacting with monocytes and macrophages that are responsible for engulfing and removing cellular debris, old cells, and unwelcome external invaders from the bloodstream. On the contrary, tumor tissues are characterized by a large vascular permeability and high interstitial diffusivity while a lack of lymphatic drainage is observed. This phenomenon is explained by the enhanced permeability and retention (EPR) effect, which significantly affects distributions of the macromolecules facilitating their access and accumulation in tumors (*30, 31*). Consequently, the micelles that accumulated in the solid tumors through the EPR effect can stay for a prolonged time. The biodistribution study, therefore, showed that the cytotoxicity of the micelles seems to depend on their retention time as well as in the accumulated amounts in each organ, which may be crucial in attaining both an effective antitumor activity and reduced toxicity in a single drug carrier system.

In vivo antitumor activity test showed that the micelles effectively suppressed tumor growth in mice over a broad range of injection doses while toxicity remained extremely low. On the other hand, the biodistribution study revealed that the micelles circulated in the blood for a long period of time and accumulated in normal organs as well as the tumors. These results are very interesting because the micelles showed organ-dependent differences in cytotoxicity. To elucidate this, we investigated the localization of the micelles in each organ by calculating the tissue-to-blood concentration ratio K_b (Table 4). The K_b value is defined as $[K_b = C_{tissue}/C_{blood}]$ where C_{tissue} and C_{blood} denote the tissue concentration and the blood concentration of the micelles, respectively. Each K_b value indicates distribution of the micelles in vascular space ($K_b < 0.1$), extracellular space ($0.1 < K_b < 0.5$), and intracellular space ($0.5 < K_b$) (*32, 33*). The data revealed that the micelles localized in the cell interior of tumor tissues but mainly distributed in the extracellular space of other organs after accumulation. It is in good accordance with our previous results published elsewhere (*34, 35*). We speculate that such drastic alterations might be due to the pathological differences in vasculatures and lymphatic drainages between organs. Consequently, even though the micelles accumulate in normal organs, they can be excreted from the body before releasing drugs. The organ-dependent cytotoxicity of the micelles, therefore, probably would depend on their retention time as well as the accumulated amounts in each organ.

The Micelles Regulate the Local Drug Distribution within Solid Tumors. In view of their tumor-specific accumulation and intracellular distribution, the micelles should release the drugs in solid tumors along with emitting fluorescence as we observed in the intracellular drug release experiment using MCTS. In contrast, if the micelles released the drugs slowly or not at all, the fluorescence of ADR would remain quenched. On the basis of this hypothesis, we observed the solid tumors and their peripheral blood vessels in mice after intravenous injection of the micelles using a fluorescence microscope (Figure 6B). The observations were carried out at 24 h after injection because the micelles needed to

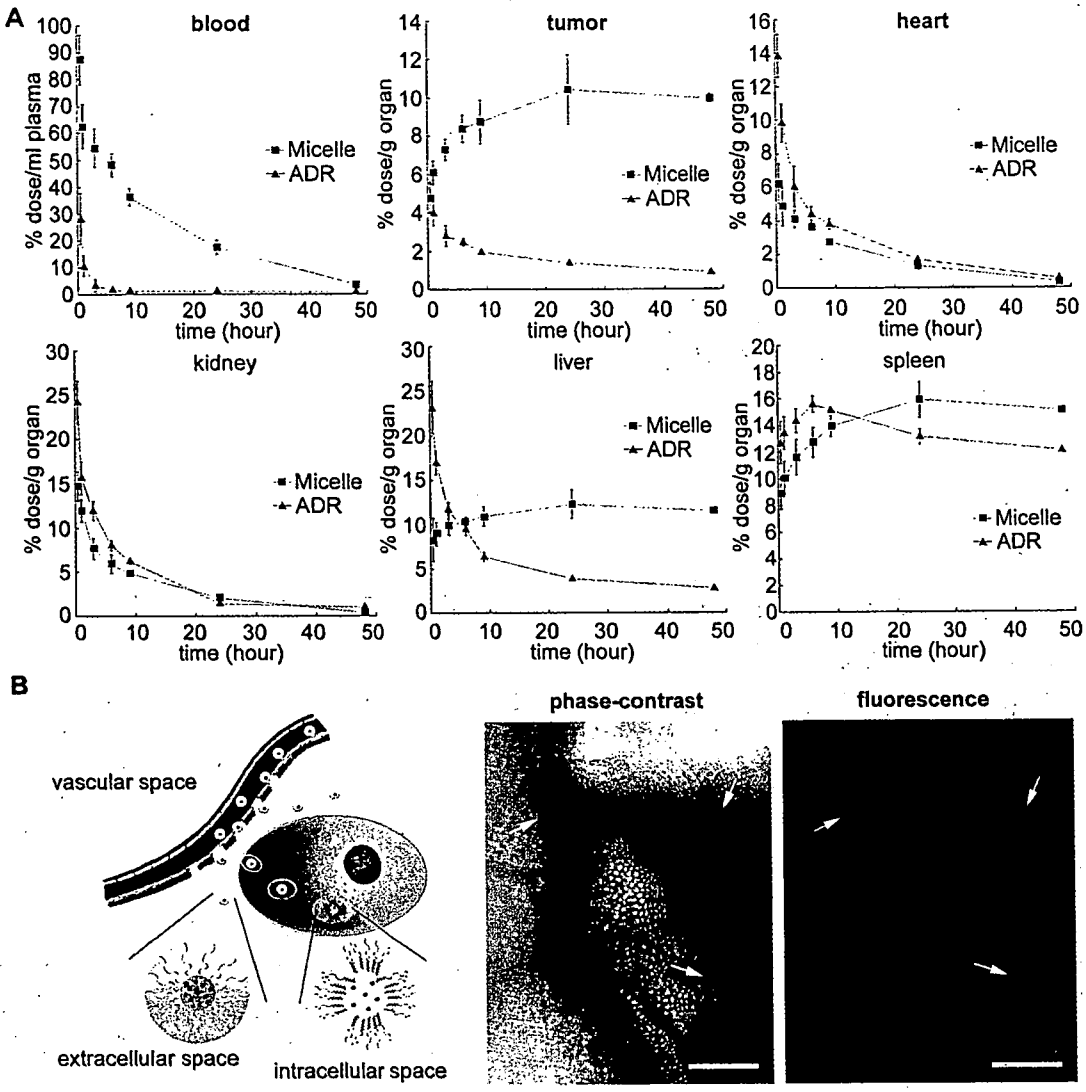

Figure 6. Tumor-specific accumulation of the micelles and locally increased drug concentrations. (A) Biodistribution study revealed the prolonged circulation in the blood and tumor-specific accumulation of the micelles. (B) Fluorescence microscopic observations of the solid tumor and its peripheral regions at 24 h after micelle injection demonstrate that the drug concentrations in the tumor tissues selectively increased due to the tumor-specific accumulation and controlled drug release from the micelles (bar = 500 μm).

Table 3. Tumor-Specific Accumulation of the Micelles

	AUC[a]		AUC ratio	tumor selectivity[b] (AUC_{tumor}/AUC_{organ})		tumor selectivity ratio $[(AUC_{tumor}/AUC_{organ})_{micelle}/(AUC_{tumor}/AUC_{organ})_{ADR}]$
	ADR	micelle	($AUC_{micelle}/AUC_{ADR}$)	ADR	micelle	
blood	58.86	858.54	14.59	–	–	–
tumor	49.59	210.21	4.24	–	–	–
heart	94.70	65.24	0.69	0.52	3.22	6.19
kidney	151.56	117.80	0.78	0.33	1.78	5.39
liver	176.15	261.17	1.48	0.28	0.80	2.86
spleen	341.38	329.66	0.97	0.15	0.64	4.27

[a] AUC denotes the area under a concentration curve that is obtained from the biodistribution study. Values are calculated based on the trapezoidal rule up to 24 h after intravenous injection. [b] Tumor selectivity of ADR and the micelles was determined by calculating the relative accumulated concentrations between the tumor tissues and each organ (AUC_{tumor}/AUC_{organ}). Their ratios indicate the change in the tumor selectivity of the micelles with respect to ADR.

accumulate in the tumor tissues enter the cells and release the drugs intracellularly as long as they were present in the blood. A phase-contrast image showed that the tumor blood vessels containing the micelles begin to leak into the extravascular compartment of the solid tumors (note the red color of the micelles). However, no fluorescence was detected at the corresponding part but in the limited regions of the solid tumor. Therefore, even though colloidal drug carriers are generally considered to localize in the limited peripheral regions of the solid tumors due to poor accessibility, we have confirmed that the micelles can infiltrate into tumor tissues after accumulation, thus increasing the local drug concentration. This conclusion is in good accordance with the results from the permeability testing of the micelles into MCTS.

DISCUSSION

This paper has revealed a new potency of the polymeric micelle drug carrier systems that they can directly deliver drugs to the interior of targeted cells in vivo by infiltrat-

Table 4. Tissue-to-blood Concentration Ratio (K_b) in Each Organ[a]

	organ				
time (h)	tumor	heart	kidney	liver	spleen
0.5	0.0545	0.0714	0.168	0.0946	0.1023
1	0.0976	0.0772	0.1903	0.1429	0.1617
3	0.134	0.0755	0.1402	0.1834	0.2136
6	0.1747	0.0764	0.1226	0.2141	0.2651
9	0.2412	0.0762	0.134	0.3014	0.3859
24	0.5992	0.0761	0.1162	0.7037	0.9158

[a] K_b value is defined as [$K_b = C_{tissue}/C_{blood}$] where C_{tissue} and C_{blood} were the tissue concentration and the blood concentration of the micelles, respectively. Each K_b value indicates the distribution of the drugs in vascular space ($K_b < 0.1$), extracellular space ($0.1 < K_b < 0.5$), and intracellular space ($0.5 < K_b$).

ing into solid tumors. These findings provided a clear answer to the questions whether the nanosized supramolecular drug carriers can access the cells in the avascular region of the solid tumors without structural and functional breakdown, which is also crucial to other intracellular environment-sensitive macromolecular bioconjugates that are injected through the vein for tumor targeting.

For the past several decades, natural and artificial macromolecules have evolved into a very useful class of drug delivery media (*36*–*39*). However, their in vivo applications are not always successful because limited accessibility inside solid tumors causes stagnation of drug carriers at the periphery of the tumor vasculatures, inducing low concentrations of active drugs in the targeted tumor tissues (*40*). Such a poor delivery efficiency of active drugs to the solid tumors is considered a serious problem facing recent cancer therapy using drug carriers. In this regard, we considered that the intrinsic characteristics of drug carriers may play a critical role in determining their in vivo behaviors, such as tumor permeability, drug release property, and antitumor activity. To confirm this, a suitable carrier model is required that controls the release of drugs while its structural features are optimized for a tumor-targeting drug delivery, and we prepared a new type of drug carrier in this study by adding an intracellular pH-triggered drug release property to the polymeric micelle drug carrier system whose chemical and biological properties are clearly identified (*41*).

As shown in the experimental results, the prepared micelle behaves not only as a biocompatible nanosized drug carrier with a high drug-loading content but also as a bioresponsive device with intracellular pH-sensitivity to control the drug release. These characteristic behaviors suggest that the nanosized core–shell structure of the micelles seems important to take the best advantage of the PEG shielding, imparting both stability and fragility into a single carrier system. The micelles safely protect the loaded drugs and functional linkers by providing a nanocompartment in the core that is completely segregated from the external environments; they maintain a high water-solubility with the hydrophilic shell that prevents the adsorption of proteins and the adhesion of cells so as to circumvent the uptake by reticuloendothelial systems during blood circulation (*42*, *43*). In the meantime, intracellular trafficking of the micelles in the solid tumors is evident, which indicates that PEG shielding of the micelle may behave as a kinetic barrier that regulates the condition of the molecular affinity interaction between the micelles and cell membrane according to the exposure or retention time. As explained by the EPR effect, solid tumors feature a large vascular permeability, high interstitial diffusivity, and poor lymphatic drainage; this is a fact that results in tumor-specific retention over a long period of time required for interacting with tumor cells. The retention time in each organ influences the intracellular trafficking of the micelles; thereby, any undesirable cytotoxicity to the normal organs is avoided. Consequently, the intracellular pH-triggered drug release property of the micelles should be the major reason for in vivo antitumor activity with low toxicity.

In conclusion, the intracellular pH-sensitive polymeric micelles exemplify the supramolecular drug carriers that control the systemic, local, and subcellular distribution of the active drugs. They show a higher bioavailability than free drugs, and therefore, the intracellular delivery of drugs would be the most effective and promising formulation for cancer chemotherapy with enhanced therapeutic efficacy and low toxicity. Moreover, the study reveals that the biocompatible structure and environment-sensitive functionality should be considered as a single event in order to realize the carrier systems that are related to these intracellular environments and material transports for the future treatment of cancers with avascular tumor tissue.

ACKNOWLEDGMENT

This research was supported by a Grant-in-Aid for Scientific Research from the Ministry of Education, Culture, Sports, Science and Technology (MEXT), Japan, and by Core Research for Evolutional Science and Technology (CREST), Japan Science and Technology Corporation (JST).

Supporting Information Available: Synthetic scheme for PEG-p(Asp-Hyd-ADR) block copolymer. HPLC analysis protocol for biodistribution. This material is available free of charge via the Internet at http://pubs.acs.org.

LITERATURE CITED

(1) Duncan, R. (2003) The dawning era of polymer therapeutics. *Nat. Rev. Drug Discovery 2*, 347–360.
(2) Maeda, H. (2001) SMANCS and polymer-conjugated macromolecular drugs advantages in cancer chemotherapy. *Adv. Drug Delivery Rev. 46*, 169–185.
(3) Jain, R. K. (2001) Delivery of molecular and cellular medicine to solid tumors. *Adv. Drug Delivery Rev. 46*, 149–168.
(4) Kopecek, J. (2003) Smart and genetically engineered biomaterials and drug delivery systems. *Eur. J. Pharm. Sci. 20*, 1–16.
(5) Nishiyama, N., Okazaki, S., Cabral, H., Miyamoto, M., Kato, Y., Sugiyama, Y., Nishio, K. Matsumura, Y., and Kataoka, K. (2003) Novel cisplatin-incorporated polymeric micelles can eradicate solid tumors in mice. *Cancer Res. 63*, 8977–8983.
(6) Lewanski, C. R. I., and Stewart, S. (1999) PEGylated liposomal adriamycin: a review of current and future applications. *Pharm. Sci. Technol. Today 2*, 473–477.
(7) Jensen, K. D., Nori, A., Tijerina, M., Kopeckova, P., and Kopecek, J. (2003) Cytoplasmic delivery and nuclear targeting of synthetic macromolecules. *J. Controlled Release 87*, 89–105.
(8) Lian, T., and Ho, R. J. Y. (2001) Trends and developments in liposome drug delivery systems. *J. Pharm. Sci. 90*, 667–680.
(9) Kataoka, K., Kwon, G., Yokoyama, M., Okano, T., and Sakurai, Y. (1993) Block-copolymer micelles as vehicles for drug delivery. *J. Controlled Release 24*, 119–132.
(10) Ringsdorf, H. (1975) Structure and properties of pharmacologically active polymers. *J. Polym. Sci. Polym. Symp. 51*, 135–153.

(11) Vasey, P. A., Kaye, S. B., Morrison, R., Twelves, C., Wilson, P., Duncan, R., Thomson, A. H., Murray, L. S., Hilditch, T. E., Murray, T., Burtles, S., Fraier, D., Frigerio, E., and Cassidy, J. (1999) Phase I clinical and pharmacokinetic study of PK1 [N-(2-hydroxypropyl)methacrylamide copolymer doxorubicin]: first member of a new class of chemotherapeutic agents – drug-polymer conjugates. *Clin. Cancer Res. 5*, 83–94.
(12) Gordon, A. N., Fleagle, J. T., Guthrie, D., Parkin, D. E., Gore, M. E., and Lacave, A. J. (2001) Recurrent epithelial ovarian carcinoma: a randomized phase III study of pegylated liposomal doxorubicin versus topotecan. *J. Clin. Oncol. 19*, 3312–3322.
(13) Nakanishi, T., Fukushima, S., Okamoto, K., Suzuki, M., Matsumura, Y., Yokoyama, M., Okano, T., Sakurai, Y., and Kataoka, K. (2001) Development of the polymer micelle carrier system for doxorubicin. *J. Controlled Release 74*, 295–302.
(14) Jain, R. K. (1994) Barriers to drug delivery in solid tumors. *Sci. Am. 271*, 58–65.
(15) Takakura, Y., and Hashida, M. (1996) Macromolecular carrier systems for targeted drug delivery: Pharmacokinetic considerations on biodistribution. *Pharm. Res. 13*, 820–831.
(16) Dvorak, H. F., Nagy, J. A., Dvorak, J. T., and Dvorak, A. M. (1998) Identification and characterization of the blood vessels of solid tumors that are leaky to circulating macromolecules. *Am. J. Pathol. 133*, 95–109.
(17) Ishida, T., Kirchmeier, M. J., Moase, E. H., Zalipsky, S., and Allen, T. M. (2001) Targeted delivery and triggered release of liposomal doxorubicin enhances cytotoxicity against human B lymphoma cells. *Biochim. Biophys. Acta Biomembranes 1515*, 144–158.
(18) Tsukioka, Y., Matsumura, Y., Hamaguchi, T., Koike, H., Moriyasu, F., and Kakizoe, T. (2002) Pharmaceutical and biomedical differences between micellar doxorubicin (NK911) and liposomal doxorubicin (Doxil). *Jpn. J. Cancer Res. 93*, 1145–1153.
(19) Unezaki. S., Maruyama, K., Hosoda, J., Nagae, I., Koyanagi, Y., Nakata, M., Ishida, O., Iwatsuru, M., and Tsuchiya, S. (1996) Direct measurement of the extravasation of poly(ethyleneglycol)-coated liposomes into solid tumor tissue by in vivo fluorescence microscopy. *Int. J. Pharm. 144*, 11–17.
(20) Suzuki, H., Nakai, D., Seita, T., and Sugiyama, Y. (1996) Design of a drug delivery system for targeting based on pharmacokinetic consideration. *Adv. Drug Delivery Rev. 19*, 335–357.
(21) Jones, A. T., Gumbleton, M., and Duncan, R. (2003) Understanding endocytic pathways and intracellular trafficking: a prerequisite for effective design of advanced drug delivery systems. *Adv. Drug Delivery Rev. 55*, 1353–1357.
(22) Bae, Y., Fukushima, S., Harada, A., and Kataoka, K. (2003) Design of environment-sensitive supramolecular assemblies for intracellular drug delivery: polymeric micelles that are responsive to intracellular pH change. *Angew. Chem., Int. Ed. 42*, 4640–4643.
(23) D'souza, A. J. M., and Topp, E. M. (2004) Release from polymeric prodrugs: linkages and their degradation. *J. Pharm. Sci. 93*, 1962–1979.
(24) Ulbrich, K., and Subr, V. (2004) Polymeric anticancer drugs with pH-controlled activation. *Adv. Drug Delivery Rev. 56*, 1023–1050.
(25) Willner, D., Trail, P. A., Hofstead, S. J., King, H. D., Lasch, S. J., Braslawsky, G. R., Greenfield, R. S., Kaneko, T., Firestone, R. A. (1993) (6-Maleimidocaproyl)hydrazone of doxorubicin. A new derivative for the preparation of immunoconjugates of doxorubicin. *Bioconjugate Chem. 4*, 521–527.
(26) Kaneko, T., Willner, D., Monkovic, I., Knipe, J. O., Braslawsky, G. R., Greenfield, R. S., and Vyas D. M. (1991) New hydrazone derivatives of adriamycin and their immunoconjugates – a correlation between acid stability and cytotoxicity. *Bioconjugate Chem. 2*, 133–141.
(27) Hamilton, G. (1998) Multicellular spheroids as an in vitro tumor model. *Cancer Lett. 131*, 29–34.
(28) Sutherland, R. M. (1988) Cell and environment interactions in tumor microregions: the multicell spheroid model. *Science 240*, 177–184.
(29) Konerding, M. A., Fait E., and Gaumann, A. (2001) 3D microvascular architecture of pre-cancerous lesions and invasive carcinomas of the colon. *Br. J. Cancer 84*, 1354–1362.
(30) Maeda, H., Wu, J., Sawa, T., Matsumura, Y., and Hori, K. (2000) Tumor vascular permeability and the EPR effect in macromolecular therapeutics: a review. *J. Controlled Release 65*, 271–284.
(31) Matsumura, Y., and Maeda, H. (1986) A new concept of macromolecular therapeutics in cancer chemotherapy: mechanism of tumoritropic accumulation of proteins and the antitumor agent SMANCS. *Cancer Res. 46*, 6387–6392.
(32) Jain, R. K. (1988) Determinants of tumor blood flow: a review. *Cancer Res. 48*, 2641–2658.
(33) Baxter, L. T., Daniel, H. Z., Mackensen, G., and Jain, R. K. (1994) Physiologically based pharmacokinetic model for specific and nonspecific monoclonal antibodies and fragments in normal tissues and human tumor xenografts in nude mice. *Cancer Res. 54*, 1517–1528.
(34) Yamamoto, Y., Nagasaki, Y., Kato, Y., Sugiyama, Y., and Kataoka, K. (2001) Long-circulating poly(ethylene glycol)-poly(D, L-lactide) block copolymer micelles with modulated surface charge. *J. Control. Release 77*, 27–38.
(35) Nishiyama, N., Kato, Y., Sugiyama, Y., and Kataoka, K. (2001) Cisplatin-loaded polymer–metal complex micelle with time-modulated decaying property as a novel drug delivery system. *Pharmaceut. Res. 18*, 1035–1041.
(36) Torchilin, V. P., Lukyanov, A. N., Gao, Z. G., and Papahadjopoulos-Sternberg, B. (2003) Immunomicelles: Targeted pharmaceutical carriers for poorly soluble drugs. *P. Natl. Acad. Sci. USA. 100*, 6039–6044.
(37) Adams, M. L., Lavasanifar, A., and Kwon, G. (2003) Amphiphilic block copolymers for drug delivery. *J. Pharm. Sci. 92*, 1343–1355.
(38) Shiah, J. G., Dvorak, M., Kopeckova, P., Sun, Y., Peterson, C. M., and Kopecek, J. (2001) Biodistribution and antitumour efficacy of long-circulating N-(2-hydroxypropyl)methacrylamide copolymer-doxorubicin conjugates in nude mice. *Eur. J. Cancer 37*, 131–139.
(39) Kopecek, J., Kopeckova, P., Minko, T., Lu, Z. R., and Peterson, C. M. (2001) Water soluble polymers in tumor targeted delivery. *J. Controlled Release 74*, 147–158.
(40) Emanuel, N., Kedar, E., Bolotin, E. M., Smorodinsky, N. I., and Barenholz, Y. (1996) Targeted delivery of doxorubicin via sterically stabilized immunoliposomes: Pharmacokinetics and biodistribution in tumor-bearing mice. *Pharm. Res. 13*, 861–868.
(41) Kataoka, K., Harada, A., and Nagasaki, Y. (2001) Block copolymer micelles for drug delivery: design, characterization and biological significance. *Adv. Drug. Delivery Rev. 47*, 113–131.
(42) Yokoyama, M., Okano, T., Sakurai, Y., Fukushima, S., Okamoto, K., and Kataoka, K. (1999) Selective delivery of adriamycin to a solid tumor using a polymeric micelle carrier system. *J. Drug Target. 7*, 171–186.
(43) Kwon, G., Suwa, S., Yokoyama, M., Okano, T., Sakurai, Y., and Kataoka, K. (1994) Enhanced tumor accumulation and prolonged circulation times of micelle-forming poly(ethylene oxide-aspartate) block copolymer-adriamycin conjugates. *J. Controlled Release 29*, 17–23.

BC0498166

British Journal of Cancer (2005) 92, 1240–1246
© 2005 Cancer Research UK All rights reserved 0007–0920/05 $30.00
www.bjcancer.com

NK105, a paclitaxel-incorporating micellar nanoparticle formulation, can extend *in vivo* antitumour activity and reduce the neurotoxicity of paclitaxel

T Hamaguchi[1], Y Matsumura[*,1,2], M Suzuki[3], K Shimizu[3], R Goda[3], I Nakamura[3], I Nakatomi[4], M Yokoyama[5], K Kataoka[6] and T Kakizoe[7]

[1]Department of Medicine, President of National Cancer Center, 5-1-1 Tsukiji, Chuo-ku, Tokyo 104-0045, Japan; [2]Investigative Treatment Division, National Cancer Center Research Institute East, 6-5-1 Kashiwanoha, Kashiwa, Chiba 277-8577, Japan; [3]Pharmaceuticals Group, Research & Development Division, Nippon Kayaku Co., Ltd, 3-31-12 Shimo, Kita-ku, Tokyo 115-8588, Japan; [4]NanoCarrier Co., Ltd, Tokatsu Techno Plaza, 5-4-6 Kashiwanoha, Kashiwa, Chiba 277-0882, Japan; [5]Kanagawa Academy of Science and Technology, KSP Bldg., East 404, 3-2-1 Sakado, Takatsu-ku, Kawasaki, Kanagawa 213-0012, Japan; [6]Department of Materials Engineering, Graduate School of Engineering, The University of Tokyo, 7-3-1 Hongo, Bunkyo-ku, Tokyo 113-8656, Japan; [7]President of National Cancer Center, 5-1-1 Tsukiji, Chuo-ku, Tokyo 104-0045, Japan

Paclitaxel (PTX) is one of the most effective anticancer agents. In clinical practice, however, high incidences of adverse reactions of the drug, for example, neurotoxicity, myelosuppression, and allergic reactions, have been reported. NK105, a micellar nanoparticle formulation, was developed to overcome these problems and to enhance the antitumour activity of PTX. Via the self-association process, PTX was incorporated into the inner core of the micelle system by physical entrapment through hydrophobic interactions between the drug and the well-designed block copolymers for PTX. NK105 was compared with free PTX with respect to their *in vitro* cytotoxicity, *in vivo* antitumour activity, pharmacokinetics, pharmacodynamics, and neurotoxicity. Consequently, the plasma area under the curve (AUC) values were approximately 90-fold higher for NK105 than for free PTX because the leakage of PTX from normal blood vessels was minimal and its capture by the reticuloendothelial system minimised. Thus, the tumour AUC value was 25-fold higher for NK105 than for free PTX. NK105 showed significantly potent antitumour activity on a human colorectal cancer cell line HT-29 xenograft as compared with PTX ($P<0.001$) because the enhanced accumulation of the drug in the tumour has occurred, probably followed by its effective and sustained release from micellar nanoparticles. Neurotoxicity was significantly weaker with NK105 than with free PTX. The neurotoxicity of PTX was attenuated by NK105, which was demonstrated by both histopathological ($P<0.001$) and physiological ($P<0.05$) methods for the first time. The present study suggests that NK105 warrants a clinical trial for patients with metastatic solid tumours.
British Journal of Cancer (2005) **92,** 1240–1246. doi:10.1038/sj.bjc.6602479 www.bjcancer.com
Published online 22 March 2005
© 2005 Cancer Research UK

Keywords: NK105; paclitaxel; polymer micelles; DDS; EPR effect

Translational Therapeutics

Paclitaxel (PTX) is one of the most useful anticancer agents known for various cancers including ovarian, breast, and lung cancers (Carney, 1996; Khayat *et al*, 2000). However, PTX has serious adverse effects, for example, neutropenia and peripheral sensory neuropathy. In addition, anaphylaxis and other severe hypersensitive reactions have been reported to develop in 2–4% of patients receiving the drug even after premedication with antiallergic agents; these adverse reactions have been attributed to the mixture of Cremophor EL and ethanol, which was used to solubilise PTX (Weiss *et al*, 1990; Rowinsky and Donehower, 1995). Of the adverse reactions, neutropenia can be prevented or managed effectively by administering a granulocyte colony-stimulating factor. On the other hand, there are no effective therapies to prevent or reduce nerve damage, which is associated with peripheral neuropathy caused by PTX; therefore, neurotoxicity constitutes a significant dose-limiting toxicity of the drug (Rowinsky *et al*, 1993; Wasserheit *et al*, 1996).

The above problems of PTX have been attributed to its low therapeutic indices and limited efficacy due to the nonselective nature of its therapeutic targets and its inability to accumulate selectively in cancer tissue. Therefore, there is an urgent need to develop modalities by which cytotoxic drugs can selectively target tumour tissue and effectively act on cancer cells in the scene. The roles of drug delivery systems (DDSs) have drawn attention in this context. Drug delivery systems are based on two main principles: active and passive targetings. The former refers to the development of monoclonal antibodies directed against tumour-related molecules that allow targeting of the tumour because of specific binding between the antibody and its antigen. However, the application of

*Correspondence: Dr Y Matsumura, Investigative Treatment Division, National Cancer Center Research Institute East, 6-5-1 Kashiwanoha, Kashiwa, Chiba 277-8577, Japan; E-mail: yhmatsum@east.ncc.go.jp
Received 27 October 2004; revised 26 January 2005; accepted 31 January 2005; published online 22 March 2005

DDSs using monoclonal antibodies is restricted to tumours expressing high levels of related antigens.

Passive targeting is based on the so-called enhanced permeability and retention (EPR) effect (Matsumura and Maeda, 1986; Maeda *et al*, 2000). The EPR effect consists in the pathophysiological characteristics of solid tumour tissue: hypervascularity, incomplete vascular architecture, secretion of vascular permeability factors stimulating extravasation within cancer tissue, and absence of effective lymphatic drainage from tumours that impedes the efficient clearance of macromolecules accumulated in solid tumour tissues.

Several techniques to maximally use the EPR effect have been developed, that is, modification of drug structures and development of drug carriers. The first micelle-forming polymeric drug developed was polyethylene glycol (PEG)-polyaspartate block copolymer conjugated with doxorubicin (DXR) (Yokoyama *et al*, 1990; Yokoyama *et al*, 1991; Kataoka *et al*, 1993). PEG constituted the outer shell of the micelle, which conferred a stealth property on the drug that allowed the micellar drug preparations to be less avidly taken up by the reticuloendothelial system (RES) and to be retained in the circulation for a longer time. Prolonged circulation time and the ability of polymeric micelles to extravasate through the leaky tumour vasculature were expected to result in the accumulation of DXR in tumour tissue due to the EPR effect (Kwon *et al*, 1994; Yokoyama *et al*, 1999). A clinical trail of micellar DXR, NK911, is now underway (Nakanishi *et al*, 2001; Hamaguchi *et al*, 2003). Recently, we succeeded in constructing NK105, a polymeric micelle carrier system for PTX, which conferred on PTX a passive targeting ability based on the EPR effect. In the present paper, we describe the details and characteristics of NK105. We also discuss differences between NK105 and other DDS formulations containing PTX.

MATERIALS AND METHODS

Materials

PTX was purchased from Mercian Corp. (Tokyo, Japan). All other chemicals were of reagent grade. Following cell lines, MKN-45, MKN-28, HT-29, DLD-1, HCT116, TE-1, TE-8, PC-14, PC-14/TXT, H460, MCAS, OVCAR-3, AsPC-1, PAN-9, PAN-3, and MCF-7 cells were purchased from American Type Culture Collection. Colon 26 cells were dispensed from the Japan Foundation for Cancer Research (Tokyo, Japan). Female BALB/c *nu/nu* mice were purchased from SLC (Shizuoka, Japan). Female CDF1 mice and IGS rats were purchased from Charles River Japan Inc. (Kanagawa, Japan).

All animal procedures were performed in compliance with the guidelines for the care and use of experimental animals, which had been drawn up by the Committee for Animal Experimentation of the National Cancer Center; these guidelines meet the ethical standards required by law and also comply with the guidelines for the use of experimental animals in Japan.

NK105, a PTX-incorporating micellar nanoparticle formulation

NK105 is a PTX-incorporating 'core-shell-type' polymeric micellar nanoparticle formulation. Polymeric micellar particles were formed by facilitating the self-association of amphiphilic block copolymers in an aqueous medium. Novel amphiphilic block copolymers, namely NK105 polymers, were designed for PTX entrapment. NK105 polymers were constructed using PEG as the hydrophilic segment and modified polyaspartate as the hydrophobic segment. Carboxylic groups of polyaspartate block were modified with 4-phenyl-1-butanol by esterification reaction, consequently the half of the groups were converted to 4-phenyl-1-butanolate. Via the self-association process, PTX was incorporated into the inner core of the micelle system by physical entrapment through hydrophobic interactions between the drug and specifically well-designed block copolymers for PTX.

Pharmacokinetics and pharmacodynamics of PTX and NK105

Colon 26 tumour-bearing CDF1 mice aged 8 weeks were given intravenously (i.v.) via the tail vein PTX 50 and 100 mg kg^{-1} or NK105 at corresponding PTX-equivalent doses. Mice were killed at 5 and 30 min, as well as 2, 6, 24, and 72 h after injection. Blood was collected, and tumours were removed; plasma and tumours obtained were then stored at −20°C until the analysis. Each time point for collection represented three samples from three different mice. PTX was extracted from plasma obtained by deproteinisation using acetonitrile, followed by liquid–liquid extraction with *t*-butylmethylether. Tumours obtained were homogenised in 0.5% acetic acid, and the resultant homogenate was deproteinised and extracted according to the same method as that used for plasma. The blood and tumour extracts were analysed for PTX by liquid chromatography/tandem mass spectrometry. Reversed-phase column-switching chromatography was conducted using an ODS column and detection was enabled by electrospray ionisation of positive mode. The mean plasma and tumour concentrations of PTX at each sampling point were calculated for both PTX and NK105. Pharmacokinetic modelling was completed using a WinNonlin Standard software version 3.1 (Pharsight Corp., California, USA).

In vitro cytotoxicity

Various human cancer cell lines were evaluated in the present study. The cell lines were maintained in monolayer cultures in Dulbecco's modified Eagle's medium containing 10% (v v^{-1}) foetal calf serum and 600 mg l^{-1} glutamine. WST-8 Cell Counting Kit-8 (Dojindo, Kumamoto, Japan) was used for the cell proliferation assay. In all, 2000 cells of each cell line in 90 μl of culture medium were plated in 96-well plates and were then incubated for 24 h at 37°C. Serial dilutions of PTX or NK105 in a volume of 10 μl were added, and the cells were incubated for 48 or 72 h. All data were expressed as mean ± s.e. of triplicate cultures. The data were then plotted as a percentage of the data from the control cultures, which were treated identically to the experimental cultures, except that no drug was added.

Evaluation of the antitumour activity of PTX and NK105

The antitumour activity of PTX and NK105 was evaluated using nude mice implanted with a human colonic cancer cell line, HT-29. One million tumour cells of HT-29 were inoculated at a subcutaneous (s.c.) site on the back skin of BALB/c female nude mice aged 6 weeks. When tumour size reached approximately 5–8 mm in diameter, mice were randomly allocated to the PTX administration group, NK105 administration group, and control administration group, each of which was made up of five animals. Each treatment was carried out as follows: free PTX group was administered at a dose of 25, 50, or 100 mg kg^{-1}; NK105 group was with same PTX-equivalent doses; and in control group, animals were given saline. Mice were administered a single i.v. injection of PTX or NK105 weekly for 3 weeks. The antitumour activity of PTX and NK105 was evaluated by measuring tumour size ($a \times b$, where a is the major diameter and b is the minor diameter) at various time points after injection. Changes in body weight were also monitored for mice, which were used in the present study.

© 2005 Cancer Research UK

Evaluation of neurotoxicity

The severity of neurotoxicity was assessed both electrophysiologically and histologically. Under intraperitoneal ketamine anaesthesia (40 mg kg^{-1}), rats were given a single i.v. injection of PTX (7.5 mg kg^{-1}), NK105 (a PTX-equivalent dose of 7.5 mg kg^{-1}), or 5% glucose weekly for 6 weeks. All the solutions were administered through the jugular vein exposed via a small incision in the neck. Electrophysiological measurements were conducted 1 day before the first dosing and on day 6 after the final dosing. For electrophysiological recording, rats were anaesthetised by the intraperitoneal injection of pentobarbital 40 mg kg^{-1}. Electrical stimuli were given peripherally, and caudal sensory nerve action potentials (caudal SNAPs) were recorded centrally from the tail. The amplitude of each waveform was calculated by measuring the caudal SNAP from the top peak to the bottom peak. Variations in the amplitude after the 6th weekly administration of the solutions were determined.

For light microscopy, rats were killed after electrophysiological recordings. Subsequently, a segment of the sciatic nerve was carefully removed, and embedded in paraffin. Sections (2 μm thick) were stained with haematoxylin and eosin (H & E) before examination under light microscopy to evaluate the degenerative changes of myelinated nerve fibres.

Statistical analysis

The data of therapeutic efficacy was expressed as mean $\pm$ s.e.m. The statistical significance of differences in therapeutic efficacy between two administration groups was calculated by means of repeated measures (analysis of variance). The statistical significance of the differences in neurotoxic activity between two administration groups was calculated using the Student's *t*-test on the closed testing procedure. The histopathological impairment was scored in five grades. The statistical significance of the differences in histopathological impairment between two administration groups was calculated using the Wilcoxon's rank-sum test on the closed testing procedure. All data were calculated with software StatView, version 5 (ABACUS Concepts, Berkeley, CA, USA). A value of $P<0.05$ was considered statistically significant.

RESULTS

Preparation and characterisation of NK105

To construct NK105 micellar nanoparticles (Figure 1A), block copolymers consisting of PEG and polyaspartate, the so-called PEG polyaspartate described previously (9, 11, 13, 14), were used. PTX was incorporated into polymeric micelles formed by physical entrapment utilising hydrophobic interactions between PTX and the block copolymer polyaspartate chain. After screening of many candidate substances, 4-phenyl-1-butanol was employed for the chemical modification of the polyaspartate block to increase its hydrophobicity. Treating with a condensing agent, 1,3-diisopropylcarbodiimide, the half of carboxyl groups on the polyaspartate, was esterified with 4-phenyl-1-butanol. Molecular weight of the polymers was determined to be approximately 20 000 (PEG block: 12 000; modified polyaspartate block: 8000). NK105 was prepared by facilitating the self-association of NK105 polymers and PTX. NK105 was obtained as a freeze-dried formulation and contained ca. 23% (w w^{-1}) of PTX, as determined by reversed-phase liquid chromatography using an ODS column with mobile phase consisting of acetonitrile and water (9:11, v v^{-1}) and detection of ultraviolet absorbance at 227 nm. Finally, NK105, a PTX-incorporating polymeric micellar nanoparticle formulation with a single and narrow size distribution, was obtained. The weight-average diameter of the nanoparticles was approximately 85 nm ranging from 20 to 430 nm (Figure 1B).

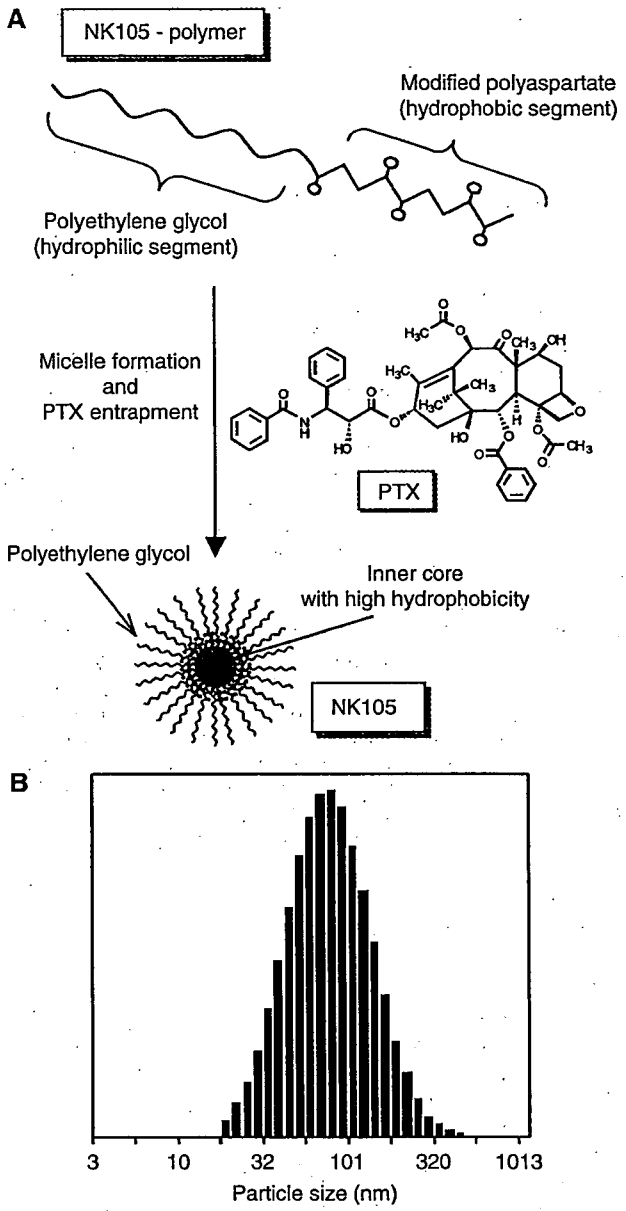

Figure 1 Preparation and characterisation of NK105. (**A**) The micellar structure of NK105 PTX was incorporated into the inner core of the micelle. (**B**) The size distribution of NK105 measured by the dynamic light scattering method. The mean diameter of an NK105 micelle was 85 nm.

Pharmacokinetics and pharmacodynamics of NK105

Colon 26-bearing CDF1 mice were given a single i.v. injection of PTX 50 or 100 mg kg^{-1}, or of NK105 at an equivalent dose of PTX. Subsequently, the time-course changes in the plasma and tumour levels of PTX were determined in the PTX and NK105 administration groups (Figure 2); furthermore, the pharmacokinetic parameters of each group were also determined (Table 1). NK105 exhibited slower clearance from the plasma than PTX, while NK105 was present in the plasma for up to 72 h after injection; PTX was not detected after 24 h or later of injection. The plasma concentration at 5 min ($C_{5\,min}$) and the area under the curve (AUC) of NK105 were 11–20-fold and 50–86-fold higher for NK105 than for PTX, respectively. Furthermore, the half-life at the terminal phase ($t_{1/2z}$) was 4–6 times longer for NK105 than for

© 2005 Cancer Research UK

PTX. The maximum concentration (C_{max}) and AUC of NK105 in Colon 26 tumours were approximately 3 and 25 times higher for NK105 than for PTX, respectively. NK105 continued to accumulate in the tumours until 72 h after injection. The tumour PTX concentration was higher than 10 $\mu g\,g^{-1}$ even at 72 h after the i.v. injection of NK105 50 and 100 $mg\,kg^{-1}$. On the contrary, the tumour PTX concentrations at 72 h after the i.v. administration of free PTX 50 and 100 $mg\,kg^{-1}$ were below detection limits and less than 0.1 $\mu g\,g^{-1}$, respectively.

In vitro cytotoxicity

NK105 was tested on 12 human tumour cell lines derived from lung, gastric, oesophagus, colon, breast, and ovarian tumours. Similar dose–response curves were noted for PTX and NK105 (data not shown). Furthermore, the IC_{50} values of NK105 were similar to those of PTX at 48 and 72 h, indicating that both NK105 and PTX showed equivalent cytotoxic activity *in vitro* (Table 2).

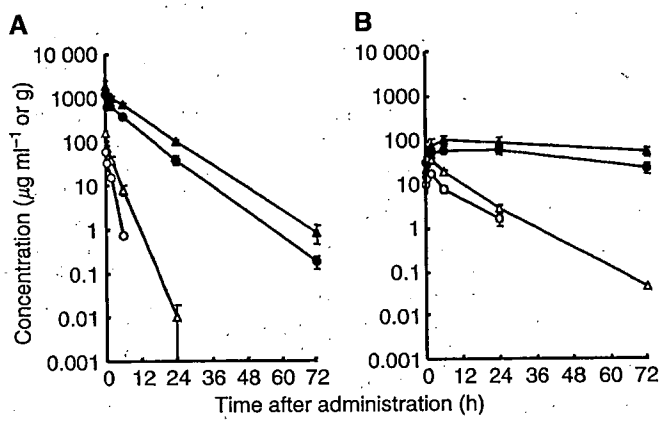

Figure 2 Plasma and tumour concentrations of PTX after single i.v. administration of NK105 or PTX to Colon 26-bearing CDF1 mice. Plasma (**A**) and tumour (**B**) concentrations of PTX after NK105 administration at a PTX-equivalent dose of 50 $mg\,kg^{-1}$ (●), NK105 at a PTX-equivalent dose of 100 $mg\,kg^{-1}$ (▲), PTX 50 $mg\,kg^{-1}$ (○) and PTX 100 $mg\,kg^{-1}$ (△).

In vivo antitumour activity

BALB/c mice bearing s.c. HT-29 colon cancer tumours showed decreased tumour growth rates after the administration of PTX and NK105. However, NK105 exhibited superior antitumour activity as compared with PTX ($P<0.001$). The antitumour activity of NK105 administered at a PTX-equivalent dose of 25 $mg\,kg^{-1}$ was comparable to that obtained after the administration of free PTX 100 $mg\,kg^{-1}$. Tumour suppression by NK105 increased in a dose-dependent manner. Tumours disappeared after the first dosing to mice treated with NK105 at a PTX-equivalent dose of 100 $mg\,kg^{-1}$, and all mice remained tumour-free thereafter (Figure 3A). In addition, less weight loss was induced in mice, which were given NK105 100 $mg\,kg^{-1}$ than in those that were given the same dose of free PTX (Figure 3B).

Table 2 IC_{50} values (μM) of PTX and NK105 in various cell lines

		48 h		72 h	
Cancer	**Cell line**	**NK105**	**PTX**	**NK105**	**PTX**
Oesophageal cancer	TE-1	>1.0	>1.0	0.01	0.02
	TE-8	0.02	0.02	0.01	0.01
Lung cancer	PC-14	0.01	0.01	0.01	0.01
	PC-14/TXT	0.15	0.09	0.08	0.06
	H460	ND	ND	0.03	0.01
Breast cancer	MCF-7	>1.0	>1.0	0.01	0.01
Stomach cancer	MKN-28	0.03	0.03	0.01	0.21
	MKN-45	0.02	0.07	0.01	0.02
Colon cancer	DLD-1	0.95	0.26	0.29	0.20
	HT-29	0.01	0.01	0.01	0.01
	HCT116	ND	ND	0.03	0.01
Ovarian cancer	MCAS	0.01	0.01	0.01	0.01
	OVCAR-3	>1.0	>1.0	>1.0	>1.0
Pancreatic cancer	AsPC-1	ND	ND	0.02	0.02
	PAN-9	ND	ND	0.03	0.02
	PAN-3	ND	ND	0.010	0.004

PTX = paclitaxel; ND = not done.

Table 1 Pharmacokinetic parameters for the plasma and tumour concentrations of paclitaxel after single i.v. administration of NK105 and PTX to Colon 26-bearing CDF1 mice

Treatment	Dose ($mg\,kg^{-1}$)	$C_{5\,min}$ ($\mu g\,ml^{-1}$)	$t_{1/2}z$ (h)	AUC_{0-t} ($\mu g\,h\,ml^{-1}$)	$AUC_{0-inf.}$ ($\mu g\,h\,ml^{-1}$)	CL_{tot} ($ml\,h\,kg^{-1}$)	V_{ss} ($ml\,kg^{-1}$)
Plasma							
PTX	50	59.32	0.98	90.2[a]	91.3	547.6	684.6
PTX	100	157.67	1.84	309.0[b]	309.0	323.6	812.2
NK105	50	1157.03	5.99	7860.9[c]	7862.3	6.4	46.4
NK105	100	1812.37	6.82	15565.7[c]	15573.6	6.4	54.8
		C_{max} ($\mu g\,ml^{-1}$)	T_{max} (h)	$t_{1/2}z$ (h)	AUC_{0-t} ($\mu g\,h\,ml^{-1}$)	$AUC_{0-inf.}$ ($\mu g\,h\,ml^{-1}$)	
Tumour							
PTX	50	12.50	2.0	7.02	120.8[b]	133.0	
PTX	100	28.57	0.5	8.06	330.4[c]	331.0	
NK105	50	42.45	24.0	35.07	2360.1[c]	3192.0	
NK105	100	71.09	6.0	73.66	3884.9[c]	7964.5	

i.v. = intravenous; $C_{5\,min}$ = plasma concentration at 5 min; $t_{1/2}z$ = half-life at the terminal phase; AUC = area under the curve; CL_{tot} = total body clearance; V_{ss} = volume of distribution at steady state; T_{max} = time of maximum concentration; PTX = paclitaxel. Parameters were calculated from the mean value of three or two mice by noncompartmental analysis. [a]AUC_{0-6h}. [b]AUC_{0-24h}. [c]AUC_{0-72h}.

© 2005 Cancer Research UK

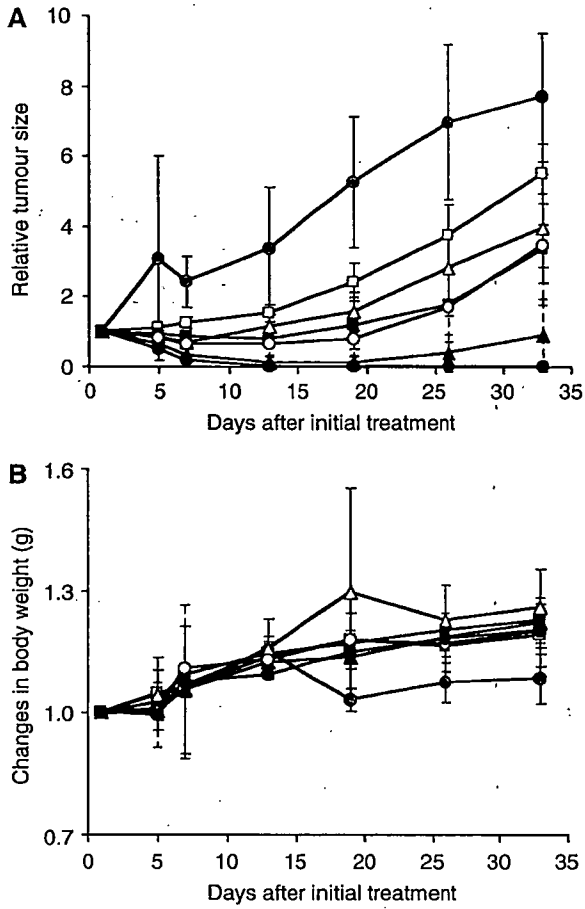

Figure 3 Relative changes in HT-29 tumour growth rates in nude mice. (**A**) Effects of PTX (open symbols) and NK105 (closed symbols). PTX and NK105 were injected i.v. once weekly for 3 weeks at PTX-equivalent doses of 25 mg kg^{-1} (□, ■), 50 mg kg^{-1} (△, ▲), and 100 mg kg^{-1} (○, ●), respectively. Saline was injected to control animals (●). (**B**) Changes in relative body weight. Data were derived from the same mice as those used for the present study.

Neurotoxicity of PTX and NK105

Treatment with PTX has resulted in cumulative sensory-dominant peripheral neurotoxicity in humans, characterised clinically by numbness and/or paraesthesia of the extremities. Pathologically, axonal swelling, vesicular degeneration, and demyelination were observed. We, therefore, examined the effects of free PTX and NK105 using both electrophysiological and morphological methods.

Prior to drug administration, there were no significant differences in the amplitude of caudal sensory nerve action potential (caudal SNAP) between two drug administration groups. On day 6 after the last dosing (at week 6), the amplitude of the caudal SNAP in the control group increased in association with rat maturation. The amplitude was significantly smaller in the PTX group than in the control group ($P<0.01$), while the amplitude was significantly larger in the NK105 group than in the PTX group ($P<0.05$) and was comparable between the NK105 group and the control group (Figure 4A). Histopathological examination of longitudinal paraffin-embedded sections of the sciatic nerve 5 days after the sixth weekly injection revealed degenerative changes. The NK105 administration group showed only a few degenerative myelinated fibres in contrast to the PTX administration group, which indicated markedly more numerous degenerative myelinated fibres ($P<0.001$) (Figure 4B and C) and Table 3.

DISCUSSION

A pharmacokinetic study revealed that the plasma AUC of NK105 was approximately 90-fold higher than that of free PTX in the present rodent models. Prolonged circulation of NK105 in the blood due to the EPR effect was associated with a significant increase in the tumour AUC. In fact, the tumour AUC of NK105 was approximately 25-fold higher than that of free PTX (Figure 2B). In mice, accordingly, NK105 exhibited stronger antitumour activity than free PTX (Figure 3A). However, it is still debatable whether or not the enhanced accumulation of an anticancer drug into a tumour is sufficient in leading the drug to exert its antitumour activity *in vivo*.

Jain *et al* have reported that the convective passage of large drug molecules into the core of solid tumours could be impeded by abnormally high interstitial pressures in solid tumours. However, they also admitted that low-molecular-weight anticancer agents might be harmful to normal organs because they can leak out of normal blood vessels freely; they finally concluded that one useful strategy for evading the barriers to drug dispersion would be to inject patients with drug carriers, such as liposomes, filled with low-molecular-weight drugs (Jain, 1994). In this case, liposomes should have sufficient time to exit from the site of tumour blood vessel leakage and to accumulate at reasonably high dose levels in the surrounding interstitium. Subsequently, low-molecular-weight drugs packed within liposomes should be released gradually so that they can be dispersed throughout the tumour. However, Unezaki *et al* have used fluorescence-labelled PEG-liposomes and described that the area of highest fluorescence was located outside tumour vessels, almost all around the vessel wall, even 2 days after drug injection (Unezaki *et al*, 1996). Therefore, the study suggested that although PEG-liposomes can be delivered effectively to a solid tumour via the EPR effect, the formulation would not be distributed sufficiently to cancer cells distant from tumour vessels because liposomes are too large to scamper about in the tumour interstitium. Liposomes have been suggested to be too stable to allow the drug therein to be released easily. Therefore, PEG-liposomes have been speculated to be not so effective against cancers in which the tumour vessel network is irregular and loose because of an abundant collagen-rich matrix. Such cancers include scirrhous cancer of the stomach and pancreatic cancer. In fact, Doxil®, a PEG-liposomal DXR, is known to be effective clinically against ovarian cancer and breast cancer, both of which are characterised by a high density of tumour microvessels; however, the drug is not effective against stomach cancer and pancreatic cancer (Muggia, 2001).

There are several possible reasons why NK105 exhibited higher antitumour activity in the present study as compared with free PTX: (1) since NK105 is very stable in the circulation and exhibits a markedly higher plasma AUC than free PTX, it accumulates better in tumour tissue than does free PTX due to the EPR effect; (2) NK105 is relatively small in size (85 nm) as compared with Doxil (100 nm), thus explaining its more uniform distribution in tumour tissue and its greater accumulation in cancer cells throughout cancer tissue. Savic *et al* (2003) have recently reported that polymeric micelles could internalise into cells to localise in several cytoplasmic organelles; and (3) a polymeric micelle carrier system for a drug has the potential to allow the effective sustained release of the drug inside a tumour following the accumulation of micelles into tumour tissue. Regarding NK105 in particular, this sustained release begins at a PTX-equivalent dose of $<1\,\mu g\,ml^{-1}$ (data not shown). Consequently, released PTX becomes distributed throughout tumour tissue and internalises into cancer cells to kill them.

© 2005 Cancer Research UK

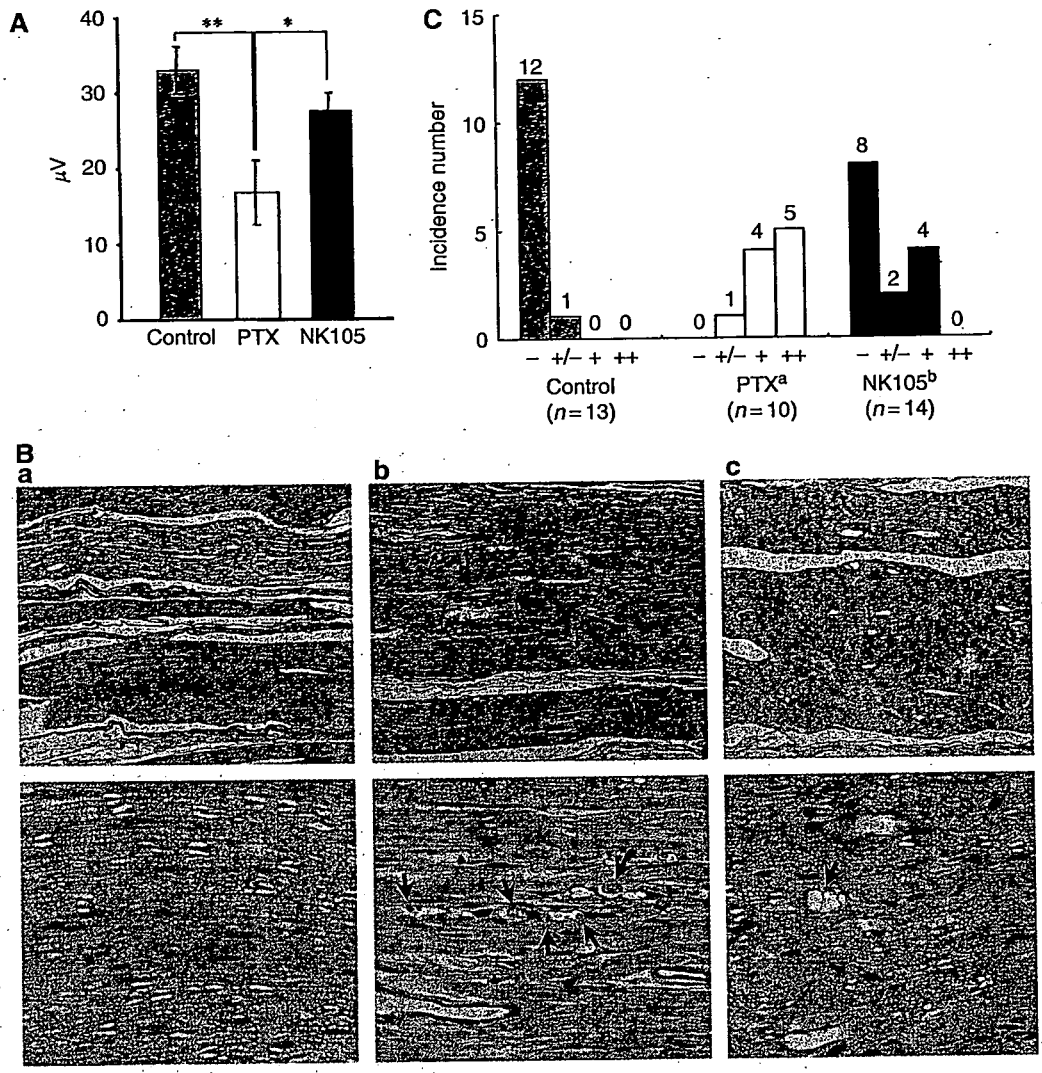

Figure 4 Incorporation of PTX into polymeric micelles diminishes neurotoxicity. (**A**) Effects of PTX or NK105 on the amplitude of rat caudal sensory nerve action potentials as examined 5 days after weekly injections for 6 weeks. Rats ($n=14$) were injected with NK105 (■) or PTX (□) at a PTX-equivalent dose of 7.5 mg kg^{-1}. Glucose (5%) was also injected in the same manner to animals in the control group (■). $^{*}P<0.05$, $^{**}P<0.01$. (**B**) Histopathological changes in the sciatic nerve of rats. Degenerating myelinated nerve fibres (arrow) were examined in the longitudinal section of the sciatic nerve (H & E) 5 days after weekly injections for 6 weeks with 5% glucose (a), PTX (b), and NK105 (c) at a PTX-equivalent dose of 7.5 mg kg^{-1}. Magnification, × 100 (upper) and × 400 (lower). (**C**) Incidences of degenerating myelinated nerve fibres in rats treated with PTX or NK105. NK105 or PTX was administered i.v. at a weekly dose of 7.5 mg kg^{-1} for 6 consecutive weeks to female rats. The degenerating myelinated fibre score was defined as follows: –, no degenerative changes; +/–, very slight degree of the degenerative changes (scattered, single fibres affected); +, slight degree of degenerative changes (scattered small groups of degenerative myelinated fibres); + +, moderate degree of degenerative changes (disseminated degenerative myelinated fibres); + + +, marked degree of degenerative changes (confluent groups of affected fibres). $^{a}P<0.001$ *vs* vehicle-treated animals. $^{b}P<0.001$ *vs* PTX-treated animals.

To date, PTX preparations that are categorised to DDSs have been developed. Among them, clinical trials are currently ongoing for the following drugs: CT-2103, polyglutamate-conjugated PTX (Singer *et al*, 2003); ABI-007, PTX coated with albumin (Ibrahim *et al*, 2002); and Genexol-PM, PTX micelle in which PTX is simply solubilised (Kim *et al*, 2004). The advantage commonly shared with these dosage forms is that they are injectable i.v. without the mixture of Cremophor EL and ethanol, which potentially provoke serious allergic reactions. The block copolymer used for forming NK105 micellar nanoparticles is nonimmunogenic and is injectable i.v. without Cremorphor EL and ethanol. Therefore, this dosage form is expected to possess a clinical advantage, which is similar to that of the above PTX dosage forms. Now, what is the difference between NK105 and other PTX dosage forms? ABI-007 and Genexol-PM were found to have the AUC and tumour AUC, which are nearly comparable or rather slightly lower than those of free PTX. Furthermore, the plasma AUC and tumour AUC are 11.5- and 11.8-fold higher, respectively, for CT-2103 than for free PTX, but they are markedly low as compared with those of NK105. Respective studies have employed proper tumours and proper rodent models. However, NK105 was forecasted to have markedly high plasma and tumour AUC as compared with those of other PTX dosage forms.

Regarding the toxicity profiles, the repeated administration of NK105 to rats at 7-day intervals produced less toxic effects on peripheral nerves than free PTX. This reduced the neurotoxicity of

© 2005 Cancer Research UK

Table 3 Incidence of degenerating myelinated fibres in rats treated with PTX or NK105

		Degenerating myelinated nerve fibre score[b]				
Treatment	***n*[a]**	**–**	**+/–**	**+**	**++**	**+++**
Control (vehicle)	13	12	1			
PTX[c]	10		1	4	5	
NK105[d]	14	8	2	4		

PTX = paclitaxel. Vehicle, NK105 or PTX was administered i.v. at a weekly dose of 7.5 mg kg^{-1} for 6 consecutive weeks to female rats. [a]Total number of animals accounted for that experimental condition. [b]Degenerating myelinated fibre score was defined as follows: –, no degenerative changes; +/–, very slight degree of the degenerative changes (scattered, single fibres affected); +, slight degree of degenerative changes (scattered small groups of degenerative myelinated fibers); ++, moderate degree of degenerative changes (disseminated degenerative myelinated fibers); +++, marked degree of degenerative changes (confluent groups of affected fibres). [c]$P<0.001$ *vs* vehicle-treated animals. [d]$P<0.001$ *vs* PTX-treated animals.

NK105, which was demonstrated for the first time by both histopathological and physiological methods and was probably attributable to the less distribution of PTX into normal neural tissue following NK105 administration, since the volume of distribution at steady state (V_{ss}) of NK105 was 100-fold lower than that of free PTX. Regarding bone marrow toxicity, there was no difference between PTX and NK105 when 37.5 mg kg^{-1} of PTX-equivalent dose was administered to rats weekly for 4 consecutive weeks (data not shown). These data indicate that NK105 warrants a clinical evaluation.

ACKNOWLEDGEMENTS

We thank Dr H Uchino, Miss M Araake, and Mrs H Koike for their technical assistance. We are also grateful to Mrs K Shiina and Miss H Orita for their secretarial assistance. This work was supported by a Grant-in-Aid from the Ministry of Health, Labor and Welfare of Japan (Y Matsumura).

REFERENCES

Carney DN (1996) Chemotherapy in the management of patients with inoperable non-small cell lung cancer. *Semin Oncol* **23:** 71–75

Hamaguchi T, Matsumura Y, Shirao Y, Shimada Y, Yamada Y, Muro Y, Okusaka T, Ueno H, Ikeda M, Watanabe N (2003) Phase I study of novel drug delivery system, NK911, a polymer micelle encapsulated doxorubicin. *Proc Am Soc Clin Oncol* **22:** 571

Ibrahim NK, Desai N, Legha S, Soon-Shiong P, Theriault RL, Rivera E, Esmaeli B, Ring SE, Bedikian A, Hortobagyi GN, Ellerhorst JA (2002) Phase I and pharmacokinetic study of ABI-007, a Cremophor-free, protein-stabilized, nanoparticle formulation of paclitaxel. *Clin Cancer Res* **8:** 1038–1044

Jain RK (1994) Barriers to drug delivery in solid tumours. *Sci Am* **271:** 58–65

Kataoka K, Kwon GS, Yokoyama M, Okano T, Sakurai Y (1993) Block copolymer micelles as vehicles for drug delivery. *J Control Rel* **24:** 119–132

Khayat D, Antoine EC, Coeffic D (2000) Taxol in the management of cancers of the breast and the ovary. *Cancer Invest* **18:** 242–260

Kim TY, Kim DW, Chung JY, Shin SG, Kim SC, Heo DS, Kim NK, Bang YJ (2004) Phase I and pharmacokinetic study of Genexol-PM, a cremophor-free, polymeric micelle-formulated paclitaxel, in patients with advanced malignancies. *Clin Cancer Res* **10:** 3708–3716

Kwon GS, Suwa S, Yokoyama M, Okano T, Sakurai Y (1994) Enhanced tumour accumulation and prolonged circulation times of micelle-forming poly(ethylene oxide-aspartic) block copolymer–adriamycin conjugate. *J Control Rel* **29:** 17–23

Maeda H, Wu J, Sawa T, Matsumura Y, Hori K (2000) Tumour vascular permeability and the EPR effect in macromolecular therapeutics: a review. *J Control Rel* **65:** 271–284

Matsumura Y, Maeda H (1986) A new concept for macromolecular therapeutics in cancer chemotherapy: mechanism of tumouritropic accumulation of proteins and the antitumour agent smancs. *Cancer Res* **46:** 6387–6392

Muggia FM (2001) Liposomal encapsulated anthracyclines: new therapeutic horizons. *Curr Oncol Rep* **3:** 156–162

Nakanishi T, Fukushima S, Okamoto K, Suzuki M, Matsumura Y, Yokoyama M, Okano T, Sakurai Y, Kataoka K (2001) Development of the polymer micelle carrier system for doxorubicin. *J Control Rel* **74:** 295–302

Rowinsky EK, Chaudhry V, Forastiere AA, Sartorius SE, Ettinger DS, Grochow LB, Lubejko BG, Cornblath DR, Donehower RC (1993) Phase I and pharmacologic study of paclitaxel and cisplatin with granulocyte colony-stimulating factor: neuromuscular toxicity is dose-limiting. *J Clin Oncol* **11:** 2010–2020

Rowinsky EK, Donehower RC (1995) Paclitaxel (taxol). *N Engl J Med* **332:** 1004–1014

Savic R, Luo L, Eisenberg A, Maysinger D (2003) Micellar nanocontainers distribute to defined cytoplasmic organelles. *Science* **300:** 615–618

Singer JW, Baker B, De Vries P, Kumar A, Shaffer S, Vawter E, Bolton M, Garzone P (2003) Poly-(L)-glutamic acid-paclitaxel (CT-2103) [XYOTAX], a biodegradable polymeric drug conjugate: characterization, preclinical pharmacology, and preliminary clinical data. *Adv Exp Med Biol* **519:** 81–99

Unezaki S, Maruyama K, Hosoda J, Nagai I, Koyanagi Y, Nakata M, Ishida O, Iwatsuru M, Tsuchiya S (1996) Direct measurement of the extravasation of polyethylene glycol-coated liposomes into solid tumour tissue by *in vivo* fluorescence microscopy. *Int J Pharmacol* **144:** 11–17

Wasserheit C, Frazein A, Oratz R, Sorich J, Downey A, Hochster H, Chachoua A, Wernz J, Zeleniuch-Jacquotte A, Blum R, Speyer J (1996) Phase II trial of paclitaxel and cisplatin in women with advanced breast cancer: an active regimen with limiting neurotoxicity. *J Clin Oncol* **14:** 1993–1999

Weiss RB, Donehower RC, Wiernik PH, Ohnuma T, Gralla RJ, Trump DL, Baker Jr JR, Van Echo DA, Von Hoff DD, Leyland-Jones B (1990) Hypersensitivity reactions from taxol. *J Clin Oncol* **8:** 1263–1268

Yokoyama M, Miyauchi M, Yamada N, Okano T, Sakurai Y, Kataoka K, Inoue S (1990) Polymer micelles as novel drug carrier:adriamycin-conjugated poly(ethylene glycol)-poly(aspartic acid) block copolymer. *J Control Rel* **11:** 269–278

Yokoyama M, Okano T, Sakurai Y, Ekimoto H, Shibazaki C, Kataoka K (1991) Toxicity and antitumour activity against solid tumours of micelle-forming polymeric anticancer drug and its extremely long circulation in blood. *Cancer Res* **51:** 3229–3236

Yokoyama M, Okano T, Sakurai Y, Fukushima S, Okamoto K, Kataoka K (1999) Selective delivery of adriamycin to a solid tumour using a polymeric micelle carrier system. *J Drug Target* **7:** 171–186

© 2005 Cancer Research UK

British Journal of Cancer (2005) 93, 678–687
© 2005 Cancer Research UK All rights reserved 0007–0920/05 $30.00
www.bjcancer.com

Cisplatin-incorporating polymeric micelles (NC-6004) can reduce nephrotoxicity and neurotoxicity of cisplatin in rats

H Uchino[1], Y Matsumura[*,1], T Negishi[1], F Koizumi[1], T Hayashi[2], T Honda[3], N Nishiyama[4], K Kataoka[4], S Naito[5] and T Kakizoe[6]

[1]Investigative Treatment Division, National Cancer Center Research Institute East, 6-5-1 Kashiwanoha, Kashiwa, Chiba 277-8577, Japan; [2]NanoCarrier Co., Ltd, 5-4-19 Kashiwanoha, Kashiwa, Chiba 277-0882, Japan; [3]Department of Anatomy and Histology, Fukushima Medical University School of Medicine, 1-Hikariga-oka, Fukushima, Fukushima 960-1247, Japan; [4]Department of Materials Science and Engineering, Graduate School of Engineering, The University of Tokyo, 7-3-1 Hongo, Bunkyo-ku, Tokyo 113-8656, Japan; [5]Department of Urology, Graduate School of Medical Sciences, Kyushu University, 3-1-1 Maidashi, Higashi-ku, Fukuoka, Fukuoka 812-8582, Japan; [6]National Cancer Center, 5-1-1 Tsukiji, Chuo-ku, Tokyo 104-0045, Japan

In spite of the clinical usefulness of cisplatin (CDDP), there are many occasions in which it is difficult to continue the administration of CDDP due to its nephrotoxicity and neurotoxicity. We examined the incorporation of CDDP into polymeric micelles to see if this allowed the resolution of these disadvantages. Cisplatin was incorporated into polymeric micelles through the polymer–metal complex formation between polyethylene glycol poly(glutamic acid) block copolymers and CDDP (NC-6004). The pharmacokinetics, pharmacodynamics, and toxicity studies of CDDP and NC-6004 were conducted in rats or mice. The particle size of NC-6004 was approximately 30 nm, with a narrow size distribution. In rats, the area under the curve and total body clearance values for NC-6004 were 65-fold and one-nineteenth the values for CDDP ($P<0.001$ and 0.01, respectively). In MKN-45-implanted mice, NC-6004 tended to show antitumour activity, which was comparable to or greater than that of CDDP. Histopathological and biochemical studies revealed that NC-6004 significantly inhibited the nephrotoxicity of CDDP. On the other hand, blood biochemistry revealed transient hepatotoxicity on day 7 after the administration of NC-6004. Furthermore, rats given CDDP showed a significant delay ($P<0.05$) in sensory nerve conduction velocity in their hind paws as compared with rats given NC-6004. Electron microscopy in rats given CDDP indicated the degeneration of the sciatic nerve, but these findings were not seen in rats given NC-6004. These results were presumably attributable to the significantly reduced accumulation of platinum in nerve tissue when NC-6004 was administered ($P<0.05$). NC-6004 preserved the antitumour activity of CDDP and reduced its nephrotoxicity and neurotoxicity, which would therefore seem to suggest that NC-6004 could allow the long-term administration of CDDP where caution against hepatic dysfunction must be exercised.

British Journal of Cancer (2005) **93,** 678–687. doi:10.1038/sj.bjc.6602772 www.bjcancer.com
Published online 13 September 2005
© 2005 Cancer Research UK

Keywords: cisplatin; polymeric micelle; EPR effect; neurotoxicity

Cisplatin (*cis*-dichlorodiammineplatinum (II): CDDP) is a key drug in the chemotherapy for cancers, including lung, gastrointestinal, and genitourinary cancer (Roth, 1996; Boulikas and Vougiouka, 2004). However, we often find that it is necessary to discontinue treatment with CDDP due to its adverse reactions, for example, nephrotoxicity and neurotoxicity, despite its persisting effects (Pinzani *et al*, 1994). Platinum (Pt) analogues, for example, carboplatin and oxaliplatin (Cleare *et al*, 1978), have been developed to date to overcome these CDDP-related disadvantages. Consequently, these analogues are becoming the standard drugs for ovarian cancer (du Bois *et al*, 2003) and colon cancer (Cassidy *et al*, 2004). However, those regimens including CDDP are considered to constitute the standard treatment for lung cancer, stomach cancer, testicular cancer (Horwich *et al*, 1997), and urothelial cancer (Bellmunt *et al*, 1997). Therefore, the development of a drug delivery system (DDS) technology is anticipated, which would offer the better selective accumulation of CDDP into solid tumours while lessening its distribution into normal tissue.

Drug delivery system targeting involves two concepts: active targeting and passive targeting. Active targeting aims drug targeting through antigen–antibody reactions and specific bindings between molecules, for example, receptor and ligand. On the other hand, passive targeting is an approach in which the drug accumulates in tumour tissue using the pathophysiological characteristics of solid tumours such as the hyperplasia of tumour vasculature which generally occurs in solid tumours, but which is not seen in a comparable way in lymph nodes. Marked vascular hyperpermeability is also found in the tumour vasculature, and the combination of hyperplasia and hyperpermeability facilitate the extravasation of high-molecular-weight polymers or nanoparticles, which are less prone to leak from intact vasculature, and which can be retained in solid tumour tissue for a longer time (enhanced permeability and retention effect (EPR) effect) (Matsumura and Maeda, 1986; Maeda and Matsumura, 1989; Maeda, 2000, 2001). This effect allows passive targeting of macromolecules with a high blood retention profile into the site of tumour.

Simple polymerisation only is not sufficient to bring about the EPR effect, and strategies are also required to suppress trapping by

*Correspondence: Dr Y Matsumura; E-mail: yhmatsum@east.ncc.go.jp
Received 13 July 2005; revised 5 August 2005; accepted 9 August 2005; published online 13 September 2005

the reticuloendothelial system (RES) and to enhance the blood retention profile (Klibanov *et al*, 1990, 1991; Allen, 1994; Gabizon *etal*, 1996; Lasic, 1996). Polyethylene glycol-tagged liposomal adriamycin (Doxil®) has recently been reported as a clinical success (Orditura *etal*, 2004). We have recently been conducting research dedicated to the development of polymeric micelles capable of incorporating anticancer drugs (Yokoyama *et al*, 1990, 1991, 1999). The Phase I clinical trial of adriamycin-incorporating polymeric micelles has been completed (Matsumura *et al*, 2004). Furthermore, in an animal model, the plasma and tumour area under the curve (AUC) values for taxol-incorporating polymeric micelle (NK105) showed 85- and 25-fold increases, respectively, as compared with those for taxol. Therefore, NK105 showed significant enhancement ($P<0.001$) of the antitumour activity of free taxol and a significant reduction ($P<0.05$) in its neurotoxicity (Hamaguchi *et al*, 2005). Based on these results, the Phase I clinical trial of NK105 is currently being conducted at the National Cancer Center Hospital, Tokyo. We have also been conducting research dedicated to the development of CDDP-incorporating polymeric micelles and have made a number of improvements, in the *in vivo* antitumour activity, reduction of nephrotoxicity, particle size, and particle size distribution as variables (Nishiyama and Kataoka, 2001; Nishiyama *et al*, 2001). Consequently, we discovered that block copolymers, which react with CDDP, acquire a long blood retention profile with the use of polyethylene glycol poly(glutamic acid) block copolymers (PEG-P(Glu)) (Nishiyama *et al*, 2003). In the present study, we used the final development of the technology to prepare CDDP-incorporating polymeric micelles (NC-6004) in an attempt to investigate the following objectives: (1) calculation of pharmacokinetic (PK) parameters in a detailed PK study of CDDP and NC-6004 in rats; (2) a comparison between CDDP and NC-6004 with respect to their antitumour activity in a human cancer cell line; and (3) a detailed comparison between CDDP and NC-6004 with respect to nephrotoxicity and neurotoxicity, which constitute the dose-limiting factors of CDDP.

MATERIALS AND METHODS

Materials

Cisplatin was purchased from WC Heraeus GmbH & Co., KG (Hanau, Germany). γ-Benzyl-L-glutamate *N*-carboxy anhydride was purchased from a supplier. *N,N*-dimethylformamide and 3-(4,5-dimethylthiazol-2-yl)-2,5-diphenyltetrazolium bromide were purchased from Wako Pure Chemical Co., Inc. (Osaka, Japan). α-Methoxy-ω-aminopropyl polyethylene glycol ($CH_3O-PEG-CH_2CH_2CH_2-NH_2$; MW = 12 000) was purchased from NOF Corporation (Tokyo, Japan).

Following cell lines, MKN-45, MKN-28, EJ-1, J82, MBT-2, colo201, colo320, HT-29, A549, EBC-1, PC-14, and MCF-7 cells were purchased from the American Type Culture Collection.

Female BALB/*c nu/nu* mice were purchased from SLC (Shizuoka, Japan). Female Sprague-Dawley rats were purchased from Charles River Japan (Kanagawa, Japan). All animal procedures were performed in compliance with the guidelines for the care and use of experimental animals, which had been drawn up by the Committee for Animal Experimentation at the National Cancer Center; these guidelines meet the ethical standards required by law and also comply with the guidelines for the use of experimental animals in Japan and the UKCCCR guidelines (UKCCCR, 1998).

Preparation of PEG-P(Glu) and preparation of CDDP-incorporating polymeric micelles (NC-6004)

Polyethylene glycol-P(Glu) block copolymers were synthesised according to the slightly modified procedure of the previously reported synthetic method of PEG-P(Asp) (Nishiyama and Kataoka, 2001). γ-Benzyl L-glutamate *N*-carboxy anhydride was polymerised in *N,N*-dimethylformamide, initiated with the NH_2 amino group of $CH_3O-PEG-CH_2CH_2CH_2NH_2$, to obtain PEG-poly(γ-benzyl L-glutamate) block copolymers (PEG-PBLG). The polymerisation degree of PBLG was determined to be 40 by comparing proton ratios between PEG ($-OCH_2CH_2-$: $\delta = 3.7$ p.p.m.) and phenyl groups of PBLG ($-CH_2C_6H_5$: $\delta = 7.3$ p.p.m.) in ^1H NMR measurement (Mercury plus 300 (Varian Technologies); solvent: DMSO-d_6; and temperature: 25°C). The benzyl group was deprotected by mixing with 0.5 N NaOH at ambient temperature to obtain PEG-P(Glu) as a sodium salt.

Cisplatin-incorporating polymeric micelles (NC-6004) were prepared according to the slightly modified procedure of the previously reported synthetic method of CDDP-incorporating polymeric micelles (Nishiyama *et al*, 2003). Briefly, the sodium salt of PEG-P(Glu) and CDDP were dissolved in distilled water ([Glu] = 4.7 mmol l^{-1}; [CDDP]/[Glu] = 1.0) and were allowed to react for 72 h. NC-6004 thus prepared was purified with ultrafiltration (molecular weight cutoff size: 100 000). The size distribution of NC-6004 was evaluated by dynamic light scattering (DLS) at 23°C using the NICOMP 380 ZLS particle sizer (Particle Sizing Systems, Santa Barbara, CA).

Release of CDDP from NC-6004 dissolved in saline

NC-6004 was dissolved in saline and was then incubated at 37°C. In all, 80 μl of the solution was then harvested at 3, 6, 24, and 96 h after the onset of incubation. The release of CDDP from NC-6004 in the solution harvested at 37°C was quantified by gel permeation chromatography (column: Waters Ultrahydrogel 500 (ϕ7.8 × 300 mm); Waters GPC system equipped with a UV detector (310 nm); and eluent: 10 mmol l^{-1} phosphate-buffered 50 mmol l^{-1} NaCl solution).

In vitro cytoxicity

Various human cancer cell lines were evaluated in the present study. The cell lines were maintained in monolayer cultures in Dulbecco's modified Eagle's medium containing 10% (v v^{-1}) focal calf serum and 600 mg l^{-1} glutamine. WST-8 Cell Counting kit-8 (Dojindo, Kumamoto, Japan) was used for cell proliferation assay. In all, 2000 cells of each cell line in 90 μl of culture medium were plated in 96-well plates and were then incubated for 24 h at 37°C. Serial dilutions of CDDP and NC-6004 in a volume of 10 μl were added, and the cells incubated for 48 or 72 h. All dates were expressed as mean ± s.e. of triplicate of the date triplicate cultures. The data were then plotted as a percentage of the data from the control cultures, which were treated identically to the experimental cultures, except that no drug was added.

Pharmacokinetics and pharmacodynamics of CDDP and NC-6004

Under isoflurane anaesthesia, a polyethylene catheter was inserted into the right internal jugular vein of female Sprague-Dawley female rats. Rats ($n = 3$) were given a single intravenous (i.v.) injection of CDDP (5 mg kg^{-1}) or NC-6004 (an equivalent dose of 5 mg kg^{-1} CDDP) via the tail vein. At 5, 15, and 30 min, as well as at 1, 4, 12, 24, and 48 h after injection of each drug, blood (0.2 ml) was collected into a heparinised microtube via the polyethylene catheter. The blood samples were centrifuged (1000 g) for 10 min at room temperature to obtain the plasma. The plasma samples were stored below −80°C until the analysis. In a tissue distribution study, rats were injected i.v. with CDDP (5 mg kg^{-1}) or NC-6004 (an equivalent dose of 5 mg kg^{-1} CDDP) via the tail vein, and were then killed in groups of three animals at 10 min, at 1, 6, 24, and 48 h, and on day 7 day after injection of each drug under intraperitoneal pentobarbital anaesthesia (50 mg kg^{-1}). Various organs (kidney, liver, spleen, heart, lung, small intestine, colon,

© 2005 Cancer Research UK

and stomach) were dissected. The organ samples were stored below −80°C until the analysis. Female BALB/*c* mice were inoculated subcutaneously on the back with 10^6 MKN-45 cells (UKCCCR, 1998). After 10 days, when the tumour size had reached approximately 50 mm^2, mice were injected i.v. with CDDP (5 mg kg^{-1}) or NC-6004 (an equivalent dose of 5 mg kg^{-1} CDDP) via the tail vein and were then killed in groups of three animals at 10 min, at 1, 6, 24, and 48 h, and on day 7 after injection of each drug. The tumours were dissected and stored below −80°C until the analysis. The plasma samples were diluted with 0.1 N HCl, vortexed, and analysed for elemental Pt by frameless atomic absorption spectrophotometry (FAAS). The tissue samples were decomposed by heating in concentrated nitric acid, evaporated to dryness, and redissolved in 0.1 N HCl. Elemental Pt was measured by FAAS.

The PK parameters were calculated using noncompartmental analysis (WinNonlin standard software, version 3.1; Pharsight Corporation, Palo Alto, CA, USA). The following PK parameters were obtained: AUC, maximum Pt concentration (C_{max}), time to obtain C_{max} (T_{max}), total body clearance (CL_{tot}), terminal half-life of Pt ($t_{1/2}z$), and steady-state volume of distribution (V_{ss}). The area under the tumour concentration-time curve (tumour AUC) was calculated based on the trapezoidal rule up to 48 h. The parameters were calculated using the following equations:

$$AUC_{0-t}$$

was calculated by the trapezoidal rule to the last measurable data point:

$$AUC_{0-inf.} = \int_0^\infty C(t)dt$$

$$t_{1/2}z(\text{terminal half-life}) = 0.693/\lambda z$$

λz: first-order rate constant associated with terminal portion of the curve)

$$CL_{tot} = \text{Dose}/AUC_{0-inf.}$$

$$V_{ss} = MRT \times CL_{tot}(MRT : \text{mean residence time})$$

In vivo antitumour activity

Antitumour activity was evaluated using nude mice implanted with a human gastric cancer cell line MKN-4. BALB/*c nu/nu* female mice (aged 6 weeks) were inoculated subcutaneously with 10^6 MKN-45 cells on the right dorsal skin. After 3 days, when tumour diameter had reached approximately 3 mm, tumour-bearing mice were allocated randomly to drug administration groups of six animals each. The drugs were administered as follows: animals in the CDDP group were given doses of 0.5, 2.5, 5 mg kg^{-1}; animals in the NC-6004 group were given doses of 0.5, 2.5, and 5 mg kg^{-1}; and animals in the control group were given the 5% glucose solution. Cisplatin or NC-6004 was administered to mice at any of the above dose levels per dose every 3 days. Antitumour activity was evaluated in terms of tumour size by measuring two orthogonal diameters ($a \times b$: a, long diameter; b, short diameter) at various time points. Animals were killed by cervical dislocation when the tumour size reached approximately 15 mm (UKCCCR, 1998). Changes in body weight were also monitored for the mice which were used in the present study.

Nephrotoxicity and hepatotoxicity of CDDP and NC-6004

Under isoflurane anaesthesia, five groups of Sprague-Dawley female rats (aged 6 weeks; 185–215 g initial body weight) were given a single i.v. injection of 5% glucose ($n=8$), CDDP at a dose of 10 mg kg^{-1} ($n=12$), NC-6004 at a dose of 10 mg kg^{-1} on a CDDP basis ($n=13$), or NC-6004 at a dose of 15 mg kg^{-1} on a CDDP basis ($n=8$). Samples of blood and major organs were taken on day 7 after administration (UKCCCR, 1998). In the case of administering NC-6004 at a dose of 10 mg kg^{-1} on a CDDP basis, five samples of blood and major organs were taken on day 14 after administration. The organs were immersed in 10% formalin solution. In each blood sample, plasma concentrations of blood urea nitrogen (BUN), creatinine, glutamic oxaloacetic transaminase (GOT), and glutamic pyruvic transaminase (GPT) were measured by SRL Laboratories (Tokyo, Japan). In addition, WBC and platelet were counted for blood samples 7 and 14 days after each drug administration in SRL Laboratories (Tokyo, Japan).

Evaluation of neurotoxicity

The severity of neurotoxicity was assessed by electrophysiological and histopathological procedures. Under isoflurane anaesthesia, rats ($n=5$) were given CDDP (2 mg kg^{-1}), NC-6004 (an equivalent dose of 2 mg kg^{-1} CDDP), or 5% glucose, all i.v., twice a week, to a total of 11 administrations. Electrophysiological measurements were conducted at week 6 after the first administration, using the method described previously (McKeage *et al*, 1994; Screnci *et al*, 2000). Under light anaesthesia with phenobarbital, responses were evoked by stimulating the sciatic nerve at its notch and the tibial nerve at the ankle of the right hind paw, using a percutaneous needle electrode. The plantar muscle H- and M-waves were recorded using a pair of superficial silver-silver chloride electrodes applied to the sole and dorsum of the hind paw. H-response-related sensory nerve conduction velocity (SNCV) was calculated by dividing the distance between the stimulation sites at the sciatic notch and ankle by the difference in H-response latency after stimulation at the ankle and sciatic notch. M-response-related motor nerve conduction velocity (MNCV) was calculated by dividing the distance between the stimulation sites at the sciatic notch and ankle by the difference in M-response latency after stimulation at the sciatic notch and ankle. At week 7 after the initial administration, rats under deep anaesthesia with phenobarbital were subjected to intracardiac catheterisation and were rinsed with saline, followed by perfusion with 4% glutaraldehyde in 0.12 M PBS. Subsequently, a segment of the sciatic nerve was carefully removed. One part of the sciatic nerve was post-fixed with 4% glutaraldehyde in 0.12 M PBS for 24 h and was then embedded in epoxy resin as described previously (Cavaletti *et al*, 1992). The remaining parts of the sciatic nerve were immersed in a 10% formalin solution. Semi-thin (1 μm thick) and thin sections were prepared from the resin-embedded sciatic nerve for light microscopic observation and electron microscopic observation, respectively.

To determine the Pt concentration in the sciatic nerve, rats were given CDDP (5 mg kg^{-1}, $n=5$), NC-6004 (an equivalent dose of 5 mg kg^{-1} CDDP, $n=5$), or 5% glucose ($n=2$), all i.v. twice a week, to a total of four administrations. On day 3 after the final administration, a segment of the sciatic nerve was removed. The removed sciatic nerve was prepared for ICP-MS analysis as described previously (Screnci *et al*, 2000). Briefly, the nerve was immersed in 1 ml of 70% nitric acid overnight. On the next day, the nerve was digested for 2 h at 90°C and Milli-Q was then added to a final volume of 5 ml. Finally, the Pt concentration in the sample solution was analysed with an ICP-MS spectrometer (SPQ 9000; Seiko Instruments Inc., Tokyo, Japan).

Statistical analysis

Data on therapeutic efficacy and body weight change were expressed as the mean ± s.e. The other data were expressed as the mean ± s.d. The statistical significance of differences in therapeutic efficacy and body weight change between two administration groups was calculated by repeated-measured

© 2005 Cancer Research UK

analysis of variance (ANOVA). The statistical significance of differences in other data between two administration groups was calculated with the Student's *t*-test. All data were calculated with StatView® Software, version 5 (ABACUS Concepts, Berkeley, CA). A value of $P<0.05$ was considered statistically significant.

RESULTS

Preparation and characterisation of CDDP-incorporating polymeric micelles (NC-6004)

Cisplatin-incorporating polymeric micelles (NC-6004) consist of CDDP and PEG–P(Glu) (Figure 1A). Furthermore, NC-6004 consists of PEG, a hydrophilic chain which constitutes the outer shell of the micelles, and the coordinate complex of P(Glu) and CDDP, a polymer–metal complex-forming chain which constitutes the inner core of the micelles. The molecular weight of PEG–P(Glu) as a sodium salt was approximately 18 000 (PEG: 12 000; P(Glu): 6000). The CDDP-incorporated polymeric micelles were clearly discriminated from typical micelles from amphiphilic block copolymers. The driving force of the formation of the CDDP-incorporated micelles is the ligand substitution of Pt(II) atom from chloride to carboxylate in the side chain of P(Glu). The molar ratio of CDDP to the carboxyl groups in the copolymers was 0.71 (Nishiyama *et al*, 2003). A narrowly distributed size of polymeric micelles (30 nm) was confirmed by the DLS measurement

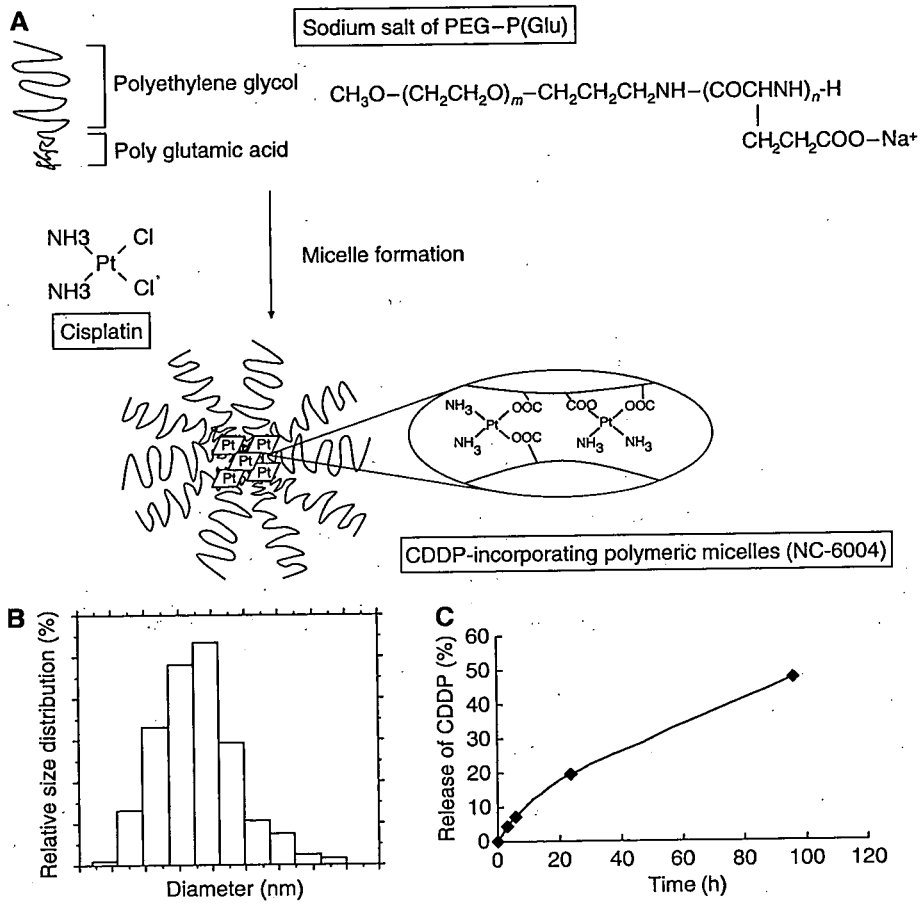

Figure 1 Preparation and characterisation of CDDP-incorporating polymeric micelles (NC-6004). (**A**) Chemical structures of CDDP and PEG–P(Glu) block copolymers, and the micellar structures of CDDP-incorporating polymeric micelles (NC-6004). (**B**) The particle size distribution of NC-6004 measured by the dynamic light-scattering method. The mean particle size of NC-6004 was approximately 30 nm. (**C**) Release of CDDP from NC-6004 in saline at 37°C.

Table 1 Pharmacokinetic parameter estimates for CDDP and NC-6004 in rats (see text for definitions of parameters)

Compound	Rat	T_{max}[a] (h)	C_{max}[a] ($\mu g\,ml^{-1}$)	$t_{1/2z}$ (h)	AUC_{0-t} ($\mu g\,h\,ml^{-1}$)	$AUC_{0-inf.}$ ($\mu g\,h\,ml^{-1}$)	CL_{tot} ($ml\,h^{-1}\,kg^{-1}$)	$MRT_{0-inf.}$ (h)	V_{ss} ($l\,kg^{-1}$)
CDDP	Mean	0.083	11.67	34.50	20.47	75.73	70.67	46.57	3.00
	s.d.		0.57	16.14	2.25	26.13	20.34	22.38	0.61
NC-6004	Mean	0.50	89.90	6.43	1325.90	1335.47	3.77	10.67	0.04
	s.d.		4.29	0.55	77.85	75.99	0.21	0.15	0.0023

The pharmacokinetic parameters were calculated after fitting to a noncompartment model using WinNonlin program. [a]For CDDP group, T_{max} represents time of maximum concentration.

© 2005 Cancer Research UK

(Figure 1B). Also, the static light scattering (SLS) measurement revealed that the CDDP-loaded micelles showed no dissociation upon dilution and the CMC was less than 5×10^{-7}, suggesting remarkable stability compared with typical micelles from amphiphilic block copolymers (Nishiyama *et al.* 1999). It is assumed that the interpolymer crosslinking by Pt(II) atom might contribute to stabilisation of the micellar structure.

The release rates of CDDP from NC-6004 were 19.6 and 47.8% at 24 and 96 h, respectively (Figure 1C). Therefore, the release of CDDP was as slow as the previously reported release (Nishiyama *et al*, 2003). In distilled water, furthermore, NC-6004 was stable without releasing CDDP (data not shown).

Pharmacokinetics and pharmacodynamics

Frameless atomic absorption spectrophotometry could measure serum concentrations of Pt up to 48 h after i.v. injection of NC-6004, but could measure them only up to 4 h after i.v. injection of CDDP. NC-6004 showed a very long blood retention profile as compared with CDDP. The AUC_{0-t} and C_{max} values were significantly higher in animals given NC-6004 than in animals given CDDP, namely, 65- and 8-fold, respectively ($P<0.001$ and 0.001, respectively) (Table 1, Figure 2A). Furthermore, the CL_{tot} and V_{ss} values were significantly lower in animals given NC-6004 than in animals given CDDP, that is, one-nineteenth and one-seventy-fifth, respectively ($P<0.01$ and 0.01, respectively) (Table 1).

Regarding the concentration–time profile of Pt in various tissues after i.v. injection of CDDP or NC-6004, all organs measured exhibited the highest concentrations of Pt within 1 h after administration in all animals given CDDP (Figure 2B). Furthermore, animals given NC-6004 exhibited the highest tissue concentrations of Pt in the liver and spleen at late time points (24 and 48 h after administration, respectively). However, the concentrations decreased on day 7 after administration (Figure 2C). In addition, and in a similar manner to other drugs which are incorporated in polymeric carriers, NC-6004 demonstrated accumulation in organs of the reticuloendothelial system, for example, liver and spleen. At 48 h after administration, tissue concentrations of Pt in the liver and spleen were 4.6- and 24.4-fold higher for NC-6004 than for CDDP. On the other hand, a marked increase in tissue Pt concentration was observed immediately after administration in the kidneys of animals given CDDP. Renal Pt concentration at 10 min and 1 h after administration were 11.6- and 3.1-fold lower, respectively, in animals given NC-6004 than in animals given CDDP. Furthermore, the maximum concentration (C_{max}) in the kidney was 3.8-fold lower at the time of NC-6004 administration than at the time of CDDP administration.

Regarding the tumour accumulation of Pt, tumour concentrations of Pt peaked at 10 min after administration of CDDP. On the other hand, tumour concentrations of Pt peaked at 48 h after administration of NC-6004 (Figure 2D). The maximum concentration (C_{max}) in tumour was 2.5-fold higher for NC-6004 than for CDDP ($P<0.001$). Furthermore, the tumour AUC was 3.6-fold higher for NC-6004 than for CDDP (81.2 and 22.6 $\mu g\,ml\,h^{-1}$ in animals given NC-6004 and CDDP, respectively).

In vitro cytotoxicity

NC-6004 was tasted on 12 human tumour cell lines derived from bladder, colon, lung, gastric, and breast cancers. The IC_{50} values of NC-6004 were 6-to 15-fold higher than those of CDDP (Table 2).

In vivo antitumour activity

BALB/*c* nude mice implanted with a human gastric cancer cell line MKN-45 showed decreased tumour growth rates after i.v. injection of CDDP and NC-6004 (Figure 3A). In the administration of CDDP,

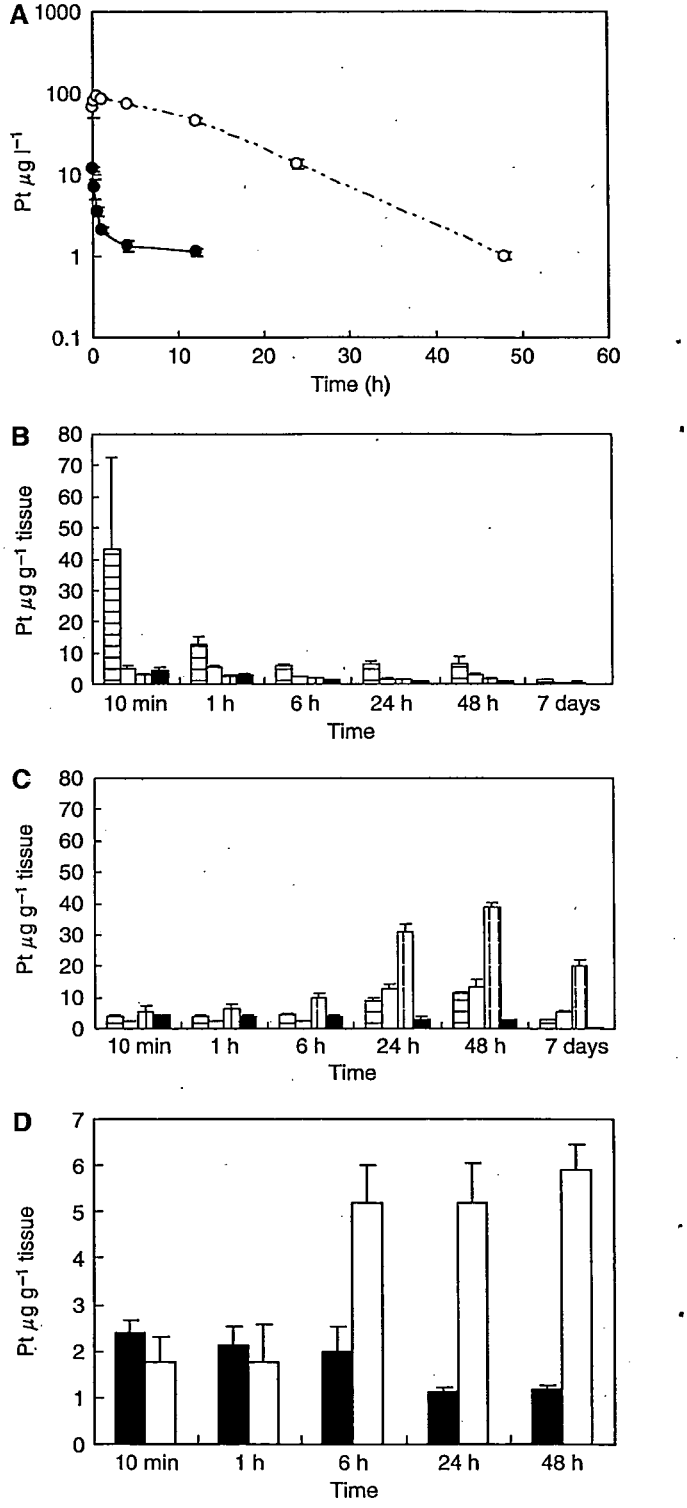

Figure 2 Time profiles of Pt concentration in the plasma and tissue distribution of Pt after a single i.v. injection of CDDP (5 $mg\,kg^{-1}$) or NC-6004 (an equivalent dose of 5 $mg\,kg^{-1}$ CDDP). (**A**) Concentration–time profile of Pt in the plasma after a single i.v. injection of CDDP (●) and NC-6004 (○) in rats ($n=3$). Tissue distribution of Pt after a single i.v. injection of CDDP (**B**) and NC-6004 (**C**) in rats ($n=3$) (kidney (▤), liver (□), spleen (▥), and lung (■)). (**D**) Time profiles of Pt concentration in the MKN-45 solid tumour after a single i.v. injection of CDDP (■) and NC-6004 (□) in MKN-45 bearing BALB/*c* nude mice ($n=3$). Values are expressed as the mean ± s.d.

© 2005 Cancer Research UK